

# Data-to-Model Distillation: Data-Efficient Learning Framework

Ahmad Sajedi<sup>1\*</sup>, Samir Khaki<sup>1\*</sup>, Lucy Z. Liu<sup>2</sup>, Ehsan Amjadian<sup>2</sup>, Yuri A. Lawryshyn<sup>1</sup>, and Konstantinos N. Plataniotis<sup>1</sup>

<sup>1</sup> University of Toronto, Toronto, Canada

<sup>2</sup> Royal Bank of Canada (RBC), Toronto, Canada

<https://datadistillation.github.io/D2M/>  
{ahmad.sajedi,samir.khaki}@mail.utoronto.ca

**Abstract.** Dataset distillation aims to distill the knowledge of a large-scale real dataset into small yet informative synthetic data such that a model trained on it performs as well as a model trained on the full dataset. Despite recent progress, existing dataset distillation methods often struggle with computational efficiency, scalability to complex high-resolution datasets, and generalizability to deep architectures. These approaches typically require retraining when the distillation ratio changes, as knowledge is embedded in raw pixels. In this paper, we propose a novel framework called Data-to-Model Distillation (D2M) to distill the real dataset’s knowledge into the learnable parameters of a pre-trained generative model by aligning rich representations extracted from real and generated images. The learned generative model can then produce informative training images for different distillation ratios and deep architectures. Extensive experiments on 15 datasets of varying resolutions show D2M’s superior performance, re-distillation efficiency, and cross-architecture generalizability. Our method effectively scales up to high-resolution  $128 \times 128$  ImageNet-1K. Furthermore, we verify D2M’s practical benefits for downstream applications in neural architecture search.

**Keywords:** Data Distillation · Efficient Training · Image Classification

## 1 Introduction

Deep learning has been successful in various domains, including computer vision and natural language processing [1, 4, 26, 33, 65, 66, 74, 82]; however, it often relies on deep neural networks (DNNs) and large-scale datasets. These requirements necessitate significant investments in training time, data storage, and electricity consumption, making training impractical for those with limited computational resources. Techniques such as pruning [34, 35, 45, 57], quantization [83, 96], and model distillation [28, 44] show promise in reducing these computational expenses while preserving performance. *Model distillation* [19, 27, 28, 60, 62, 67, 68, 89], in

---

\*Equal contribution

We include some relevant evaluation protocol material in B.

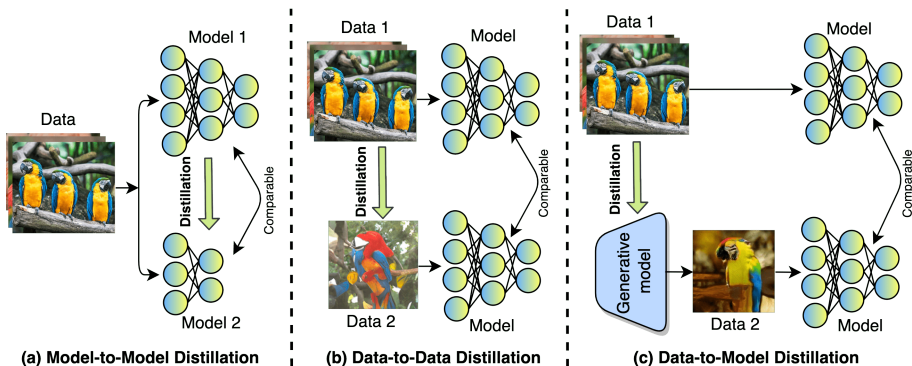


Fig. 1: Different distillation frameworks for efficient learning.

particular, transfers the informative knowledge from a large teacher model to a smaller student one to facilitate model compression (Fig. 1(a)). Recently, *dataset distillation* [5, 6, 64, 81, 90, 93, 94, 97] has emerged as a promising data-efficient learning approach that distills knowledge from a large training dataset into a small set of synthetic images. These images enable models to attain test performance comparable to those trained on the original dataset (Fig. 1(b)). Dataset distillation is widely applied in computer vision for applications like neural architecture search [29, 73], continual learning [10, 22, 64, 85, 91], federated learning [48, 50, 84], and privacy-preserving [7, 15, 53].

Traditional data-centric methods, known as *coreset selection*, reduce training costs by selecting a subset of the original dataset based on specific metrics [2, 61, 70, 75, 96]. However, these approaches have a deficiency in representation capability and coverage of chosen samples, leading to suboptimal results for classification tasks [61, 75, 96]. State-of-the-art dataset distillation algorithms overcome these limitations by synthesizing a small yet informative dataset that aligns characteristics between synthetic and real images. Drawing on seminal work [81], researchers have developed various methods, including gradient matching [18, 43, 91, 94], distribution matching [36, 64, 79, 93, 95], trajectory matching [5, 13, 17, 23], and kernel-inducing points [52, 59, 97]. These works initialize a small number of learnable images and update their raw pixel values using different matching strategies during distillation.

Existing dataset distillation studies have shown remarkable performance but suffer from three major drawbacks. First, they require complete retraining of distillation algorithms when the distillation ratio (or the number of images per class) changes, which leads to a computationally demanding re-distillation process. Second, these methods generally struggle with high-resolution, large-scale datasets (*e.g.*  $128 \times 128$  ImageNet-1K [14]) and tend to distill visually noisy images [5]. Lastly, the distilled dataset often performs poorly on architectures like ResNet [26], DenseNet [31] and ViT [16]. These issues partially stem from parameterizing the synthetic dataset in pixel space. Optimizing raw pixels can capture

high-frequency, detailed information that is not essential for downstream tasks and is susceptible to over-fitting to the training architecture [6]. Moreover, employing pixel-level optimization on high-resolution, large-scale data incurs significant computational and memory costs, rendering it unscalable for such datasets.

In this paper, we propose a novel framework, Data-to-Model distillation (D2M), that transfers information from the original dataset into a generative model rather than relying on raw pixel data (Fig. 1(c)). D2M effectively addresses the aforementioned issues by parameterizing the synthetic dataset within the parameter space of a generative model, such as Generative Adversarial Networks (GANs) [3, 21]. Following the approach of [64, 78, 95, 97], our method employs a model pool to extract rich representations that are essential for learning. We design embedding matching and prediction matching modules to minimize differences in channel attention maps (at various layers) and output predictions between real and generated images, respectively. As depicted in Fig. 2, these modules facilitate the distillation of different types of knowledge into the generative model using suitable matching losses, all geared towards improving classification performance. Following the distillation stage, our generative model can create training samples for classification tasks with *any* number of images per class from random noises. Unlike other dataset distillation methods, D2M circumvents the need for retraining the distillation when changing the distillation ratio, which offers clear advantages in re-distillation efficiency. As D2M stores information in models rather than pixels, it stands as one of the pioneer distillation methods scalable to high-resolution ( $256 \times 256$ ) and large-scale datasets. This makes it a promising tool for efficient synthetic data generation, requiring significantly less memory storage. The contributions of our study are:

**[C1]:** We propose a novel framework to distill the knowledge of large-scale datasets into a *parameter space of a generative model* that can produce informative images for classification tasks. The method distills various representations from the real data to provide diverse supervision.

**[C2]:** We conduct extensive experiments on 15 datasets, differing in resolution, label complexity, and application domains. We achieve state-of-the-art results across all settings and enable the distillation of the ImageNet-1K at a resolution of  $128 \times 128$  with a fixed storage complexity across different settings.

**[C3]:** We show that data-to-model distillation outperforms prior dataset distillation algorithms in re-distillation efficiency and cross-architecture generality. The high-quality images generated by D2M also notably improve downstream applications in neural architecture search.

## 2 Related Work

**Dataset Distillation.** Wang *et al.* [81] introduced dataset distillation to synthesize small-scale data from a large real dataset using meta-learning, minimizing training loss differences between the synthetic and original data. Meta-learning involves bi-level optimization and incurs significant computational costs. To mitigate this, researchers employed kernel methods to facilitate the inner optimiza-

tion loop, as seen in KIP [58, 59], RFAD [52], and FRePo [97]. Other studies adopted surrogate objectives to tackle unrolled optimization problems in meta-learning. DC [94], DSA [91], and IDC [37] align gradients between synthetic and real datasets for distillation. Meanwhile, DM [93], CAFE [79], DAM [64], and ATOM [36] use distribution-matching to alleviate bias caused by original samples with large gradients. Further, MTT [5], FTD [17], and TESLA [13] match model parameter trajectories to improve performance. However, these methods distill information into pixels, leading to a linear growth in computational costs with class numbers and resolutions. This limits scalability with larger datasets and poses challenges for cross-architecture generalization and re-distillation efficiency [5, 49, 64, 79, 94]. In contrast, D2M distills the knowledge into the generative model to address the limitations posed by pixel-wise dataset distillation.

**Generative Models.** This work is closely related to generative models, specifically generative adversarial networks (GANs) [21, 41, 80, 98]. Goodfellow et al. [21] introduced vanilla GANs to generate realistic images that deceive human observers. A variety of GAN models, such as CycleGAN [98], InfoGAN [9], and BigGAN [3], have since emerged for tasks like image manipulation [42, 80, 98], super-resolution [24, 41], and object detection [46, 47]. However, these GAN-generated images often prioritize visual realism over informativeness, which may not be ideal for data-efficient classification tasks [6, 78, 79, 92]. Some methods have been proposed to address this by generating samples that can be used to train deep neural networks more efficiently. GLaD [6] distills numerous images into a few intermediate feature vectors in the GAN’s latent space to help cross-architecture generalization. Wang et al. [78] introduced a two-stage algorithm for optimizing generative models to create training samples for 10-class classification tasks. Nevertheless, these methods face challenges such as high training costs [78], the necessity of retraining for different distillation ratios [6], and scalability constraints for complex, high-resolution datasets [78]. In contrast, our approach distills discriminative knowledge from the dataset into the *parameter space* of generative models, reducing re-distillation costs and achieving superior performance on standard benchmarks for both low- and high-resolution datasets.

### 3 Methodology

In this section, we introduce a novel framework called D2M, which distills knowledge from a large-scale training dataset  $\mathcal{T} = \{(\mathbf{x}_i, y_i)\}_{i=1}^{|\mathcal{T}|}$ , with  $|\mathcal{T}|$  image-label pairs, into a generative model  $G$ . In the distillation phase, we extract comprehensive knowledge from the real dataset  $\mathcal{T}$ , including embedded representations and logit prediction, and then distill them into the parameters of a pre-trained generative model. This procedure refines the generative model to synthesize a small yet informative dataset  $\mathcal{S} = \{(\mathbf{s}_j, y_j)\}_{j=1}^{|\mathcal{S}|}$  that has comparable training power to the real dataset. Following distillation, the learned generative model produces training images from random noises, enabling flexibility in the distillation ratios. These samples are subsequently deployed in classification tasks to evaluate D2M’s performance. The overall D2M pipeline is depicted in Fig. 2.

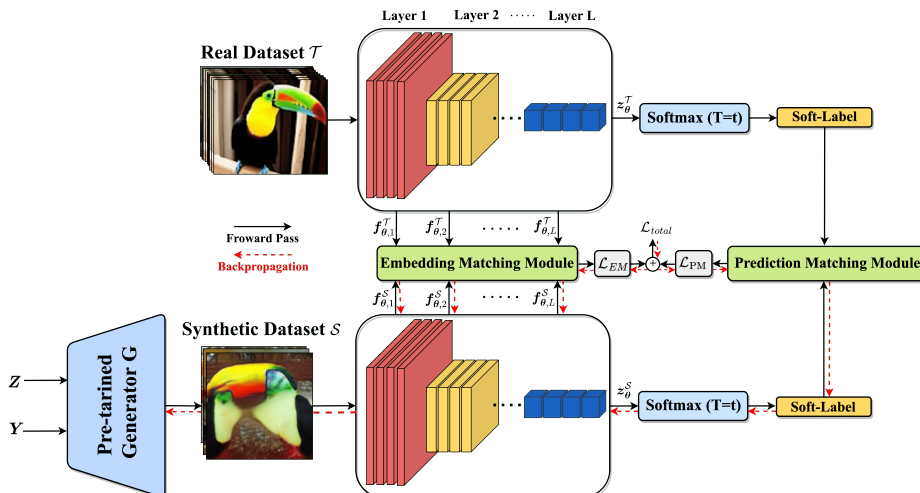


**Fig. 2:** An overview of the proposed D2M framework. D2M distills the knowledge of large-scale datasets into the parameter space of a pre-trained generator through embedding matching and prediction matching modules. The learned generator can then produce small yet informative training images for the downstream classification tasks.  $Z$  and  $Y$  represent the random noises and labels, respectively.

### 3.1 Data-to-Model Distillation

The proposed D2M differs from data distillation works that directly distill knowledge into raw pixels. In D2M, we distill the information into the learnable parameters of a generative model, offering a new path for efficient learning.

A randomly initialized generative model yields noisy outputs, making it challenging to establish meaningful correspondences with real images during the distillation process. Therefore, we employ a pre-trained Generative Adversarial Network (GAN) with a generator  $G$  and a discriminator  $D$ , trained using the following standard loss function:

$$\min_G \max_D \mathbb{E}_{\mathbf{x} \sim P_{\mathcal{T}}} [\log D(\mathbf{x}|y)] + \mathbb{E}_{\mathbf{z} \sim P_Z} [\log(1 - D(G(\mathbf{z}|y)))] \quad (1)$$

where  $P_{\mathcal{T}}$  and  $P_Z$  denote the distributions of real training images and latent vectors, respectively. As highlighted by [92], conventional GANs typically generate images that deviate from the original data distribution and are less informative than real samples for training deep networks. To mitigate this limitation, we introduce a distillation stage to refine the generative model. This refinement enables the model to synthesize images that are more discriminative and better suited to downstream classification tasks.

**Distillation Stage.** We randomly select  $B$  pairs consisting of random noises  $Z$  and labels  $Y$  in each batch. These pairs are then fed into the pre-trained generative model to produce synthetic images  $\mathcal{S}$ . Meanwhile, we also randomly

pick  $B$  real images from the original dataset  $\mathcal{T}$  with corresponding labels  $Y$ . During each iteration, both real and synthetic batches undergo a forward pass using a randomly chosen neural network  $\phi_{\theta}(\cdot)$  with different initializations from a model pool. This network is responsible for extracting features and predicting classification logits for both real and synthetic images. The network generates feature maps and predicted logits for each dataset, denoted as  $\phi_{\theta}(\mathcal{T}) = [\mathbf{f}_{\theta,1}^{\mathcal{T}}, \dots, \mathbf{f}_{\theta,L}^{\mathcal{T}}, \mathbf{z}_{\theta}^{\mathcal{T}}]$  for the real dataset and  $\phi_{\theta}(\mathcal{S}) = [\mathbf{f}_{\theta,1}^{\mathcal{S}}, \dots, \mathbf{f}_{\theta,L}^{\mathcal{S}}, \mathbf{z}_{\theta}^{\mathcal{S}}]$  for the synthetic one. The feature map  $\mathbf{f}_{\theta,l}^{\mathcal{T}}$  and logit  $\mathbf{z}_{\theta}^{\mathcal{T}}$  are multi-dimensional arrays obtained from the real dataset in the  $l^{\text{th}}$  and pre-softmax layers of the network, respectively. Similarly, feature  $\mathbf{f}_{\theta,l}^{\mathcal{S}}$  and logits  $\mathbf{z}_{\theta}^{\mathcal{S}}$  are derived from the synthetic set. We then adopt embedding matching and prediction matching modules to capture the representations of the real training set across various layers.

The embedding matching module aligns the channel-wise attention maps between the real and synthetic sets across different feature extraction layers using the loss function  $\mathcal{L}_{\text{EM}}$ , formulated as:

$$\mathbb{E}_{\theta \sim P_{\theta}} \left[ \sum_{l=1}^L \left\| \mathbb{E}_{\mathcal{T}} [\tilde{\mathbf{f}}_{\theta,l}^{\mathcal{T}}] - \mathbb{E}_{\mathcal{S}} [\tilde{\mathbf{f}}_{\theta,l}^{\mathcal{S}}] \right\|^2 \right], \quad (2)$$

where  $P_{\theta}$  is the distribution of neural network parameters and  $\tilde{\mathbf{f}}_{\theta,l}^{\mathcal{T}}$  is defined as:

$$\tilde{\mathbf{f}}_{\theta,l}^{\mathcal{T}} := \begin{cases} \mathbf{a}_{\theta,l}^{\mathcal{T}} & \text{if } l = 1, \dots, L-1 \\ \mathbf{f}_{\theta,L}^{\mathcal{T}} & \text{if } l = L, \end{cases} \quad (3)$$

in which  $\mathbf{a}_{\theta,l}^{\mathcal{T}}$  represents the vectorized channel attention maps in the  $l^{\text{th}}$  layer for the real dataset. In the same way, the  $\tilde{\mathbf{f}}_{\theta,l}^{\mathcal{S}}$  can be defined for the synthetic set. In particular, we characterize each training image through the use of channel-wise attention maps created by different layers. As noted in [8, 36], these attention maps highlight the most discriminative regions of the input image, revealing the network’s focus across various layers (early and intermediate) for obtaining information at low- and mid-level representations. The last layer of feature extraction in the neural network contains the highest-level abstract information [54]. This embedded has been shown to effectively capture semantic information from the input data [63, 93]. Thus, we leverage the mean square error loss to match the vectorized versions of the final feature maps with real and synthetic data. Our embedding matching uses the most *discriminative* regions of feature maps using the concept of attention, differing significantly from pure feature matching approaches like CAFE [79]. Notably, in cases where ground-truth data distributions are unavailable, we empirically estimate the expectation term in Eq. (2).

Although  $\mathcal{L}_{\text{EM}}$  effectively approximates large-scale real data distribution, its matching loss primarily minimizes the mean feature distance within each batch without explicitly constraining the diversity of synthetic images. Therefore, we use a complementary loss as a regularizer to provide more specific supervision. This regularization promotes similarity in the output probability predictions between the two datasets, directly influencing the results of the downstream

**Algorithm 1** Data-to-Model Distillation (D2M)**Input:** Real training dataset  $\mathcal{T} = \{(\mathbf{x}_i, y_i)\}_{i=1}^{|\mathcal{T}|}$ **Required:** Pre-trained generative model  $G$ , Latent vector set  $Z$ , Deep neural network  $\phi_\theta$  from a model pool with parameter distribution  $P_\theta$ , Learning rate  $\eta_G$ , Task balance parameter  $\lambda$ , Number of training iterations  $I$ .

- 1: **for**  $i = 1, 2, \dots, I$  **do**
- 2:   Sample  $\theta$  from  $P_\theta$
- 3:   Sample  $B$  pairs from the real dataset and the generated images of  $G(Z)$
- 4:   Compute  $\mathcal{L}_{\text{EM}}$  and  $\mathcal{L}_{\text{PM}}$  using Equations 2 and 4
- 5:   Calculate  $\mathcal{L} = \mathcal{L}_{\text{EM}} + \lambda\mathcal{L}_{\text{PM}}$
- 6:   Update the generator using  $G \leftarrow G - \eta_G \nabla_G \mathcal{L}$
- 7: **end for**

**Output:** Synthetic dataset  $\mathcal{S} = G(Z) = \{(\mathbf{s}_i, y_i)\}_{i=1}^{|\mathcal{S}|}$ 

classification task. Drawing inspiration from knowledge distillation works [28, 32, 88], we employ logit-based matching to minimize the differences in the *softened* output predictions between real and generated synthetic images. The soft-label predictions introduce additional information to the generative model that can be helpful for classification tasks [87]. The prediction matching loss  $\mathcal{L}_{\text{PM}}$  can then be written as follows:

$$\mathbb{E}_{\theta \sim P_\theta} \left[ \sum_{i=1}^B KL \left( \sigma \left( \frac{\mathbf{z}_\theta^{\mathbf{x}_i}}{T} \right), \sigma \left( \frac{\mathbf{z}_\theta^{\mathbf{s}_i}}{T} \right) \right) \right], \quad (4)$$

where KL stands for Kullback-Leibler divergence,  $\sigma(\cdot)$  denotes the softmax function, and  $\mathbf{z}_\theta^{\mathbf{x}_i}$  and  $\mathbf{z}_\theta^{\mathbf{s}_i}$  are the prediction logits for real and synthetic images sharing the same label  $y_i$ , respectively. The temperature hyperparameter  $T$  is used to generate soft-label predictions while regulating the entropy of the output distribution [28, 88]. Additional details on the impact of  $T$  are discussed in Sec. 4.3. Finally, the training loss for the D2M framework is formulated as the augmented Lagrangian of the two mentioned losses. We learn the *parameters of a generative model* by solving the following optimization problem using SGD:

$$G^* = \arg \min_G (\mathcal{L}_{\text{EM}} + \lambda\mathcal{L}_{\text{PM}}), \quad (5)$$

where  $\lambda$  serves as a Lagrangian multiplier to balance the gradients of  $\mathcal{L}_{\text{EM}}$  and  $\mathcal{L}_{\text{PM}}$ . The impact of  $\lambda$  is examined in Sec. 4.3 and a learning algorithm is summarized in Alg. 1.

**Comparing with Other Generative Prior Methods.** Recent generative-based dataset distillation methods typically distill large-scale datasets into the latent space of a specific GAN model [6, 92]. For example, GLaD [6] utilizes various intermediate feature spaces of StyleGAN-XL [69] to characterize synthetic datasets. IT-GAN [6] creates synthetic datasets in a BigGAN’s latent space [3] by initially inverting the full training set and then fine-tuning the latent representations based on the distillation objective. Both GLaD and IT-GAN necessitate

complete retraining when distillation ratios change due to their information containers, which require updates when changing the IPC. In contrast, D2M proposes a novel approach by parameterizing the synthetic dataset within the learnable *parameter space* of any generative model using our carefully designed framework. Unlike GLaD and IT-GAN, whose storage complexity grows linearly with increasing IPCs, our framework maintains a constant storage complexity across various distillation ratios. To demonstrate the efficacy of our framework, we empirically compare D2M with GLaD and IT-GAN, consistently outperforming them in all cases, as detailed in Sec. 4.2 and supplementary materials.

## 4 Experiments

### 4.1 Experimental Setup

**Datasets.** In line with prior studies, we evaluate the proposed framework across diverse image classification datasets with varying resolutions and label complexity. Our method is applied to CIFAR10/100 [38] for low-resolution data. The TinyImageNet [40] and ImageNet-1K [14] datasets are resized to  $64\times 64$  for medium-resolution ones. For high-resolution data (*i.e.*  $128\times 128$ ), we employ ImageNet-1K and its subsets—ImageNette [30], ImageWoof [30], ImageSquawk [5], ImageFruit [5], and ImageMeow [5]—each emphasizing specific categories such as assorted objects, dog breeds, birds, fruits, and cat breeds. We also use the recently introduced 10-class ImageNet-1K subsets (ImageNet-[A, B, C, D, E]) [6], which were determined through the evaluation performance of a pre-trained ResNet-50 on ImageNet-1K. Finally, we extend D2M to the medical imaging domain, focusing on high-resolution  $256\times 256$  images in DermaMNIST [86]. This dataset features dermatoscopic images of typical pigmented skin lesions. More details on the datasets can be found in the supplementary materials.

**Network Architectures.** Following recent dataset distillation works [64, 78, 97], we leverage a model pool to mitigate overfitting and offer diverse views for matching tasks. The model pool includes Depth- $n$  ConvNets [20] and ResNet-18/32 [26] with different initialization random seeds [64, 97]. To ensure diversity, we randomly select one model from the pool at each iteration. In a Depth- $n$  ConvNet,  $n$  blocks precede a fully connected layer, with each block containing a  $3\times 3$  convolutional layer (128 filters), instance normalization [77], ReLU activation, and  $2\times 2$  average pooling (stride of 2). The number of blocks depends on dataset resolution:  $n = 3, 4, 5,$  and  $6$  for  $32\times 32, 64\times 64, 128\times 128,$  and  $256\times 256,$  respectively. We initialize networks using normal initialization [25] and use BigGAN [3] as a default generative model.

**Evaluation Protocol.** Our method uniquely allows the dynamic generation of images for training. To ensure fairness with conventional studies like [64, 91, 93, 94], we first measure the end-to-end latency for training each model on the given dataset at a particular IPC. When evaluating our method, we generate images on-the-fly during downstream model training, ensuring that the total time for both generating and training matches the latency constraints set by previous works. This approach explores a tradeoff between model training and image

**Table 1:** The performance (%) comparison to priors on CIFAR and TinyImageNet. ConvNet is used for evaluation. For more details, refer to the supplementary materials.

Dataset	CIFAR-10			CIFAR-100			Tiny ImageNet		
	1	10	50	1	10	50	1	10	50
IPC Ratio %	0.02	0.2	1	0.2	2	10	0.2	2	10
Random	14.4 $\pm$ 2.0	26.0 $\pm$ 1.2	43.4 $\pm$ 1.0	4.2 $\pm$ 0.3	14.6 $\pm$ 0.5	30.0 $\pm$ 0.4	1.4 $\pm$ 0.1	5.0 $\pm$ 0.2	15.0 $\pm$ 0.4
Herding	21.5 $\pm$ 1.2	31.6 $\pm$ 0.7	40.4 $\pm$ 0.6	8.4 $\pm$ 0.3	17.3 $\pm$ 0.3	33.7 $\pm$ 0.5	2.8 $\pm$ 0.2	6.3 $\pm$ 0.2	16.7 $\pm$ 0.3
Forgetting	13.5 $\pm$ 1.2	23.3 $\pm$ 1.0	23.3 $\pm$ 1.1	4.5 $\pm$ 0.2	15.1 $\pm$ 0.3	30.5 $\pm$ 0.3	1.6 $\pm$ 0.1	5.1 $\pm$ 0.2	15.0 $\pm$ 0.3
DC [94]	28.3 $\pm$ 0.5	44.9 $\pm$ 0.5	53.9 $\pm$ 0.5	12.8 $\pm$ 0.3	25.2 $\pm$ 0.3	30.6 $\pm$ 0.6	5.3 $\pm$ 0.1	12.9 $\pm$ 0.1	12.7 $\pm$ 0.4
DSA [91]	28.8 $\pm$ 0.7	52.1 $\pm$ 0.5	60.6 $\pm$ 0.5	13.9 $\pm$ 0.3	32.3 $\pm$ 0.3	42.8 $\pm$ 0.4	6.6 $\pm$ 0.2	16.3 $\pm$ 0.2	25.3 $\pm$ 0.2
DM [93]	26.0 $\pm$ 0.8	48.9 $\pm$ 0.6	63.0 $\pm$ 0.4	11.4 $\pm$ 0.3	29.7 $\pm$ 0.3	43.6 $\pm$ 0.4	3.9 $\pm$ 0.2	12.9 $\pm$ 0.4	24.1 $\pm$ 0.3
CAFE [79]	30.3 $\pm$ 1.1	46.3 $\pm$ 0.6	55.5 $\pm$ 0.6	12.9 $\pm$ 0.3	27.8 $\pm$ 0.3	37.9 $\pm$ 0.3	-	-	-
CAFE+DSA [79]	31.6 $\pm$ 0.8	50.9 $\pm$ 0.5	62.3 $\pm$ 0.4	14.0 $\pm$ 0.3	31.5 $\pm$ 0.2	42.9 $\pm$ 0.2	-	-	-
DAM [64]	32.0 $\pm$ 1.2	54.2 $\pm$ 0.8	67.0 $\pm$ 0.4	14.5 $\pm$ 0.5	34.8 $\pm$ 0.5	49.4 $\pm$ 0.3	8.3 $\pm$ 0.4	18.7 $\pm$ 0.3	28.7 $\pm$ 0.3
ATOM [36]	34.8 $\pm$ 1.0	57.9 $\pm$ 0.7	68.8 $\pm$ 0.5	18.1 $\pm$ 0.4	35.7 $\pm$ 0.4	50.2 $\pm$ 0.3	9.1 $\pm$ 0.2	19.5 $\pm$ 0.4	29.1 $\pm$ 0.3
IDM [95]	45.6 $\pm$ 0.7	58.6 $\pm$ 0.1	67.5 $\pm$ 0.1	20.1 $\pm$ 0.3	45.1 $\pm$ 0.1	50.0 $\pm$ 0.2	10.1 $\pm$ 0.2	21.9 $\pm$ 0.2	27.7 $\pm$ 0.3
KIP [59]	49.9 $\pm$ 0.2	62.7 $\pm$ 0.3	68.6 $\pm$ 0.2	15.7 $\pm$ 0.2	28.3 $\pm$ 0.1	-	-	-	-
FRePo [97]	46.8 $\pm$ 0.7	65.5 $\pm$ 0.4	71.7 $\pm$ 0.2	28.7 $\pm$ 0.1	42.5 $\pm$ 0.2	44.3 $\pm$ 0.2	15.4 $\pm$ 0.3	25.4 $\pm$ 0.2	-
MTT [5]	46.3 $\pm$ 0.8	65.3 $\pm$ 0.7	71.6 $\pm$ 0.2	24.3 $\pm$ 0.3	40.1 $\pm$ 0.4	47.7 $\pm$ 0.2	8.8 $\pm$ 0.3	23.2 $\pm$ 0.2	28.0 $\pm$ 0.3
TESLA [13]	48.5 $\pm$ 0.8	66.4 $\pm$ 0.8	72.6 $\pm$ 0.7	24.8 $\pm$ 0.4	41.7 $\pm$ 0.3	47.9 $\pm$ 0.3	-	-	-
<b>D2M (Ours)</b>	<b>50.2<math>\pm</math>0.3</b>	<b>67.8<math>\pm</math>0.5</b>	<b>74.4<math>\pm</math>0.3</b>	<b>29.8<math>\pm</math>0.4</b>	<b>46.6<math>\pm</math>0.3</b>	<b>51.2<math>\pm</math>0.2</b>	<b>16.7<math>\pm</math>0.2</b>	<b>26.1<math>\pm</math>0.4</b>	<b>30.1<math>\pm</math>0.2</b>
Full Dataset	84.8 $\pm$ 0.1			56.2 $\pm$ 0.3			37.6 $\pm$ 0.4		

generation on the fly during evaluation. Details on the generation and training time costs are available with our source code <sup>‡</sup>. Apart from dynamic generation, we use the same ConvNet networks and optimizers as previous works for valid comparison. We also quantify the computational costs during distillation in GPU hours and the number of learnable parameters. For fairness and reproducibility, we employ publicly available datasets of baselines and train models using our experimental settings. For datasets without specific experiments, we implemented them using the released author codes. Additional implementation details are provided in the supplementary materials.

**Implementation Details.** We deploy the pre-trained BigGAN with the default hyperparameters and learning strategy outlined in [3]. In the distillation, we refine BigGAN using the SGD optimizer with a batch size of  $B = 128$  over  $K = 60$  epochs while setting the task balance  $\lambda$  and the temperature  $T$  to 100 and 4, respectively. We also apply the same set of differentiable augmentations [91] in all experiments, during distillation and evaluation. Experiments are conducted on two RTX A-6000 GPUs with 50 GB of memory. Additional hyperparameter details can be found in the supplementary materials.

## 4.2 Comparison to State-of-the-art Methods

**CIFAR and Tiny ImageNet.** We compare the proposed D2M with 3 core-set selection and 12 dataset distillation approaches on the CIFAR-10/100 [38] and Tiny ImageNet [40] datasets, as detailed in Tab. 1. D2M consistently outperforms all baselines across different settings for these low- and medium-resolution

<sup>‡</sup><https://github.com/DataDistillation/D2M>

**Table 2:** The performance comparison (%) to state-of-the-art methods on ImageNet-1K [14] and its high-resolution subsets [5].

Dataset	IPC	Random DAM [64]	GLaD [6]	TESLA [13]	FRePo [97]	<b>D2M (Ours)</b>	Full Dataset
ImageNet-1K (64×64)	1	0.5±0.1	2.0±0.1	-	7.7±0.2	7.5±0.3	<b>8.3±0.2</b>
	2	0.9±0.1	2.2±0.1	-	10.5±0.3	9.7±0.2	<b>11.1±0.2</b>
	10	3.1±0.2	6.3±0.0	-	17.8±1.3	-	<b>18.2±0.9</b>
	50	7.6±1.2	15.5±0.2	-	27.9±1.2	-	<b>28.3±1.1</b>
ImageNette	1	23.5±4.8	34.7±0.9	38.7±1.6	-	48.1±0.7	<b>49.9±0.2</b>
	10	47.7±2.4	59.4±0.4	-	-	66.5±0.8	<b>67.7±0.3</b>
ImageWoof	1	14.2±0.9	24.2±0.5	23.4±1.1	-	29.7±0.6	<b>32.3±0.4</b>
	10	27.0±1.9	34.4±0.4	-	-	42.2±0.9	<b>44.9±0.3</b>
ImageSquawk	1	21.8±0.5	36.4±0.8	35.8±1.4	-	-	<b>40.3±0.5</b>
	10	40.2±0.4	55.4±0.9	-	-	-	<b>59.8±0.2</b>

datasets. Specifically, it achieves up to 88% of CIFAR-10’s upper bound performance with only 1% of its training data and up to 70% of the upper bound with 2% of Tiny ImageNet’s training data. These results highlight the D2M framework’s robustness for data-efficient learning and its ability to distill informative knowledge for improved classification task performance.

**ImageNet-1K and Its Subsets.** ImageNet-1K [14] and its subsets are more challenging than the CIFAR-10/100 and Tiny ImageNet datasets due to their complex label spaces and higher resolutions. Consequently, memory and time constraints prevented previous data distillation works from scaling up to ImageNet-1K at high resolution [5, 17, 64, 91, 92, 97]. However, D2M overcomes this by distilling information from the original dataset into the generative model’s parameters rather than relying on complex raw pixels. This enables D2M, as one of the pioneering works to generate synthetic 128×128 ImageNet-1K images, outperforming Random by a significant margin up to 19.1% (Fig. 3). To understand how well our method performs on high-resolution images, we also extended the evaluation to three high-resolution ImageNet-1K subsets: ImageNette (assorted objects), ImageWoof (dog breeds), and ImageSquawk (birds) datasets, all with a resolution of 128×128. As shown in Tab. 2, we outperform prior works with the same model architecture across all settings. Notably, D2M improves the performance of the top competitor, FRePo, on the ImageWoof by more than 2.7%. This improvement stems from the fact that D2M effectively distills essential information from the original dataset into the generative model through channel-wise attention matching and softened output prediction alignment. Our ablation studies in Sec. 4.3 further confirm that the performance gain is directly related to the method’s ability to generate informative images.

To further evaluate our method’s effectiveness, we compare D2M to GLaD [6] using ImageNet-A to ImageNet-E, as well as ImageFruit and ImageMeow (cat breeds). It should be noted that GLaD is a plug-and-play method and can be added to existing dataset distillation studies. Tab. 3 presents an analysis of performance between D2M and GLaD when applied to previous techniques,

**Table 3:** The performance (%) comparison to prior works on  $128\times 128$  ImageNet-Subset (ImageFruit, ImageMeow, and ImageNet-[A, B, C, D, E]) with IPC1.

Methods	ImageFruit	ImageMeow	ImageNet-A	ImageNet-B	ImageNet-C	ImageNet-D	ImageNet-E
DC [94]	21.0 $\pm$ 0.9	22.0 $\pm$ 0.6	43.2 $\pm$ 0.6	47.2 $\pm$ 0.7	41.3 $\pm$ 0.7	34.3 $\pm$ 1.5	34.9 $\pm$ 1.5
DM [93]	20.4 $\pm$ 1.9	20.1 $\pm$ 1.2	39.4 $\pm$ 1.8	40.9 $\pm$ 1.7	39.0 $\pm$ 1.3	30.8 $\pm$ 0.9	27.0 $\pm$ 0.8
MTT [5]	22.4 $\pm$ 1.1	26.6 $\pm$ 0.4	51.7 $\pm$ 0.2	53.3 $\pm$ 1.0	48.0 $\pm$ 0.7	43.0 $\pm$ 0.6	39.5 $\pm$ 0.9
DC+GLaD [6]	20.7 $\pm$ 1.1	22.6 $\pm$ 0.8	44.1 $\pm$ 2.4	49.2 $\pm$ 1.1	42.0 $\pm$ 0.6	35.6 $\pm$ 0.9	35.8 $\pm$ 0.9
DM+GLaD [6]	21.8 $\pm$ 1.8	22.3 $\pm$ 1.6	41.0 $\pm$ 1.5	42.9 $\pm$ 1.9	39.4 $\pm$ 0.7	33.2 $\pm$ 1.4	30.3 $\pm$ 1.3
MTT+GLaD [6]	23.1 $\pm$ 0.4	26.0 $\pm$ 1.1	50.7 $\pm$ 0.4	51.9 $\pm$ 1.3	44.9 $\pm$ 0.4	39.9 $\pm$ 1.7	37.6 $\pm$ 0.7
<b>D2M (Ours)</b>	<b>24.4<math>\pm</math>0.5</b>	<b>28.4<math>\pm</math>0.3</b>	<b>55.2<math>\pm</math>0.2</b>	<b>56.8<math>\pm</math>0.6</b>	<b>50.4<math>\pm</math>0.4</b>	<b>45.2<math>\pm</math>0.6</b>	<b>41.6<math>\pm</math>0.8</b>

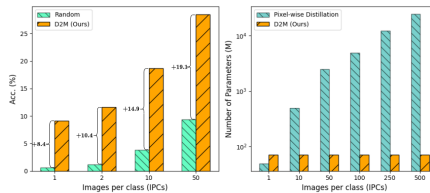
**Table 4:** GPU hours for re-distillation process from IPC1 to IPC10 and IPC50 on CIFAR-10. Total denotes the GPU hours spent on the distillation for all three IPCs.

Method	Distillation Time (GPU hours)					
	DC [94]	DSA [91]	DM [93]	MTT [5]	DAM [64]	<b>D2M</b>
IPC1	0.2	0.2	1.2	1.4	1.2	4.9
IPC1 $\rightarrow$ IPC10	1.8	2.0	1.5	7.8	1.5	<b>0</b>
IPC1 $\rightarrow$ IPC50	8.3	8.9	4.7	38.2	4.8	<b>0</b>
Total	10.3	11.1	7.4	47.4	7.5	<b>4.9</b>

namely DC [94], DM [93], and MTT [5]. In each case, we distilled a synthetic dataset with one image per class and then evaluated it on the Depth-5 ConvNet. The results show D2M’s superiority across all experimental settings.

**Higher Resolution Datasets ( $256\times 256$ ).** We extend the scaling of D2M to higher resolutions, specifically datasets with a resolution of  $256\times 256$ . To that end, we conduct experiments on two datasets: ImageSquawk and DermaMNIST. The results, shown in Tab. 6, demonstrate superior performance across both datasets, surpassing Random by a significant margin.

**Distillation Cost Analysis.** In efficient learning, it is critical to consider computational costs during the distillation. We compare the re-distillation cost and the number of learnable parameters for D2M against priors in Tab. 4 and Fig. 3, respectively. When IPCs change, previous methods require dataset re-distillation, incurring substantial computational expenses and increasing GPU hours (Tab. 4). In contrast, D2M conducts optimization on generative models’ parameters rather than raw pixels, requiring only a *single* distillation for varying IPCs. This precludes the need for repeated distillation, saving up to 42.5 GPU hours. Additionally, while the number of learnable parameters in pixel-wise data distillation increases with dataset size and resolution, D2M keeps the cost unchanged across all IPCs, saving up to 35x for IPC50, as shown in Fig. 3.

**Fig. 3:** Performance comparison and count of parameters on  $128\times 128$  ImageNet-1K.

In contrast, D2M conducts optimization on generative models’ parameters rather than raw pixels, requiring only a *single* distillation for varying IPCs. This precludes the need for repeated distillation, saving up to 42.5 GPU hours. Additionally, while the number of learnable parameters in pixel-wise data distillation increases with dataset size and resolution, D2M keeps the cost unchanged across all IPCs, saving up to 35x for IPC50, as shown in Fig. 3.

**Table 5:** Cross-architecture performance on CIFAR-10 with 50 images per class.

Method	Unseen Evaluation Architecture					Average (%)
	AlexNet [39]	VGG-11 [71]	ResNet-50 [26]	DenseNet-121 [31]	ViT [16]	
DSA [91]	53.7 $\pm$ 0.6	51.4 $\pm$ 1.0	24.4 $\pm$ 0.5	24.6 $\pm$ 1.0	43.3 $\pm$ 0.4	39.5 $\pm$ 0.7
CAFE [79]	34.0 $\pm$ 0.6	40.5 $\pm$ 0.8	46.7 $\pm$ 1.2	49.7 $\pm$ 1.3	22.7 $\pm$ 0.7	38.7 $\pm$ 0.9
MTT [5]	48.2 $\pm$ 1.0	55.4 $\pm$ 0.8	61.3 $\pm$ 0.4	62.3 $\pm$ 1.1	47.7 $\pm$ 0.6	55.0 $\pm$ 0.8
DM [93]	60.1 $\pm$ 0.5	57.4 $\pm$ 0.8	51.5 $\pm$ 0.4	58.9 $\pm$ 0.7	45.2 $\pm$ 0.4	54.6 $\pm$ 0.6
FTD [17]	53.8 $\pm$ 0.9	58.4 $\pm$ 1.6	59.9 $\pm$ 1.3	58.3 $\pm$ 1.5	49.3 $\pm$ 0.7	55.9 $\pm$ 1.2
DAM [64]	63.9 $\pm$ 0.9	64.8 $\pm$ 0.5	59.6 $\pm$ 0.8	62.2 $\pm$ 0.4	48.2 $\pm$ 0.8	59.7 $\pm$ 0.7
<b>D2M (Ours)</b>	<b>65.4<math>\pm</math>0.7</b>	<b>67.3<math>\pm</math>0.5</b>	<b>64.8<math>\pm</math>0.6</b>	<b>66.1<math>\pm</math>0.5</b>	<b>54.7<math>\pm</math>0.6</b>	<b>63.6<math>\pm</math>0.6</b>

### 4.3 Ablation Studies and Analysis

**Cross-Architecture Generalization.** Building on prior studies [5, 64, 79, 93, 94], we evaluate the ability of D2M-generated images for understanding classification tasks without overfitting to a specific architecture. We use distillation methods to create synthetic data with a default network and evaluate their performance on unseen architectures. Following the settings of [17, 64], we experiment on the CIFAR-10 dataset with IPC 50 and test generalization with architectures like AlexNet [39], VGG-11 [71], ResNet-50 [26], DenseNet-121 [31], and ViT [16]. The findings in Tab. 5 show that synthetic images from D2M not only generalize well across various models but also outperform the best competitor on average up to a margin of 3.9%. D2M illustrates the robustness of vision transformers and complex architectures like ResNet-50 and DenseNet-121 due to its powerful generative capability and distilled knowledge. This suggests D2M can identify crucial learning features beyond mere knowledge matching.

**Exploring the effect of temperature  $T$  in D2M.** In our framework, soft label predictions enrich the information in the generated synthetic dataset. Inspired by [28, 62], we use a temperature parameter  $T$  to control the entropy of the output distribution while generating soft label predictions. This ablation explores the impact of temperature on overall performance. As shown in Fig. 6(a), increasing the  $T$  value improves D2M’s performance up to a certain point ( $T = 4$ ). A lower temperature emphasizes only maximal logits, while a higher value flattens the distribution, focusing on different logits uniformly. Tuning the softmax temperature allows soft labels to reveal extra knowledge like class relationships for training, enabling information flow across classes (*dark knowledge* [28]).

**Evaluation of task balance  $\lambda$  in D2M.** In the D2M framework, we train the generative model by minimizing a linear combination of embedded-based and prediction-based matching losses, as expressed in Eq. (5). The parameter  $\lambda$  serves as the regularizing coefficient, determining the balance between the losses. In Fig. 6(c), we study different values of  $\lambda$  (ranging from 0.01 to 1000) on the CIFAR10 dataset with IPC10 to assess its sensitivity. Our default value of  $\lambda = 10$  yields the best results. Values that are too high, such as 1000, reduce the effectiveness of embedding matching, resulting in a loss of informative knowledge. Conversely, too small values compromise regularization and impede the distillation of discriminative label knowledge, which is beneficial for classification tasks.

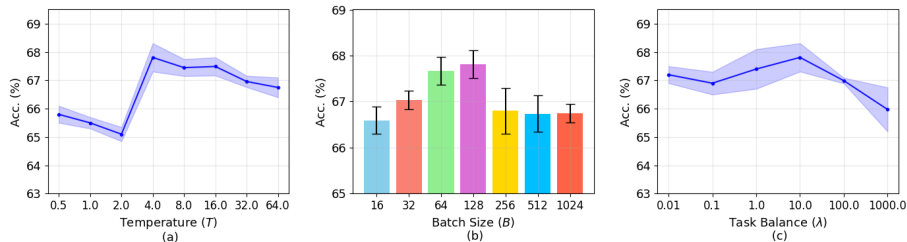


**Fig. 4:** The effect of (a) temperature, (b) batch size, and (c) task balance on the D2M’s performance for CIFAR10 with IPC10.

**Exploring the effect of loss components in D2M.** We conduct an experiment to evaluate the effect of loss components,  $\mathcal{L}_{EM}$  and  $\mathcal{L}_{PM}$ , on D2M’s performance. Conventional generative models strive to produce real-looking images but may lack the informative value of real images for training due to inherent information loss [64, 79, 93]. We refine these generators during distillation with different loss designs and observe improvements of 10.3% and 7.9% for  $\mathcal{L}_{EM}$  and  $\mathcal{L}_{PM}$ , respectively, on CIFAR10 with IPC10. This enhancement is attributed to the transfer of informative and discriminative knowledge for classification tasks. Moreover, combining  $\mathcal{L}_{EM}$  and  $\mathcal{L}_{PM}$  led to a remarkable 12.7% improvement.

**Table 6:** The performance comparison for high-resolution ( $256 \times 256$ ) datasets.

Dataset	IPC	Random	D2M
ImageSquawk	1	22.3 $\pm$ 0.5	<b>48.2<math>\pm</math>0.4</b>
	10	41.3 $\pm$ 0.6	<b>63.4<math>\pm</math>0.3</b>
DermaMNIST	1	21.3 $\pm$ 1.3	<b>46.4<math>\pm</math>0.4</b>
	10	38.4 $\pm$ 1.1	<b>67.2<math>\pm</math>0.3</b>

**Table 7:** The effect of different generators on D2M’s performance for the CIFAR10 dataset.

IPC	1	10	50
CGAN	49.6 $\pm$ 0.7	67.4 $\pm$ 0.3	72.2 $\pm$ 0.8
BigGAN	50.2 $\pm$ 0.2	67.8 $\pm$ 0.5	74.4 $\pm$ 0.3
StyleGAN-XL	<b>50.7<math>\pm</math>0.5</b>	<b>68.2<math>\pm</math>0.4</b>	<b>75.2<math>\pm</math>0.4</b>
CVAE	49.8 $\pm$ 0.3	67.6 $\pm$ 0.2	73.1 $\pm$ 0.4

**Evaluation of different generative models in D2M.** We investigate the effect of different pre-trained generators on D2M by deploying BigGAN [3], CGAN [56], StyleGAN-XL [69], and a CVAE model [11, 72] on CIFAR-10 with IPC1, 10, and 50. Tab. 7 demonstrates that all models effectively synthesize images for classification, with StyleGAN-XL outperforming the rest. However, BigGAN was chosen as the default due to its balance of performance and computational efficiency. Details on the computational costs are given in the supplementary.

#### 4.4 Visualization and Application

**Synthetic Images.** We visualize synthetic images for various datasets and resolutions in Fig. 5. These images are identifiable, although they may contain artificial patterns that improve their informativeness, like discriminative features of the animals. Note that our generative model prioritizes informativeness over realism. More visualizations are available in the supplementary materials.

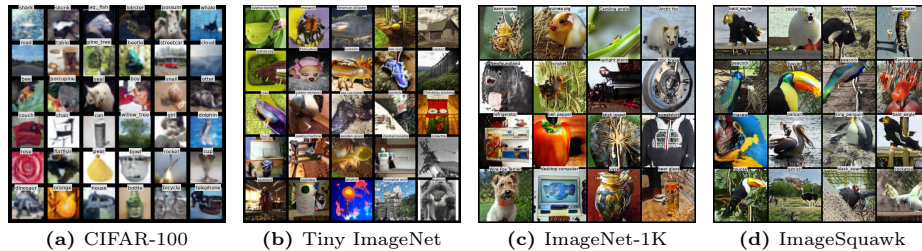


**Fig. 5:** Example generated images from  $32 \times 32$  CIFAR-100,  $64 \times 64$  Tiny ImageNet,  $128 \times 128$  ImageNet-1K, and  $128 \times 128$  ImageSquawk.

**Table 8:** Neural architecture search on the CIFAR-10 dataset.

	Random	DSA [91]	DM [93]	DAM [64]	CAFE [79]	<b>D2M (Ours)</b>	Whole Dataset
Performance (%)	88.9	87.2	87.2	88.8	83.6	<b>88.9</b>	89.2
Correlation	0.70	0.66	0.71	0.72	0.59	<b>0.80</b>	1.00
Time cost (min)	206.4	206.4	206.6	206.4	206.4	206.5	5168.9
Number of Images	<b>500</b>	<b>500</b>	<b>500</b>	<b>500</b>	<b>500</b>	<b>500</b>	$5 \times 10^4$

**Neural Architecture Search.** The synthetic images can act as a proxy set to accelerate model evaluation in the Neural Architecture Search (NAS). Following [64, 94], we conduct NAS on CIFAR-10 with a search space of 720 ConvNets, varying in network depth, width, activation, normalization, and pooling layers. More implementation details can be found in the supplementary materials. We train all architectures on the Random, DSA, CAFE, DM, DAM, and D2M synthetic sets with IPC50 for 200 epochs and on the full dataset for 100 epochs to establish a baseline. We rank architectures based on validation performance and report the testing accuracy of the best-selected model when trained on the test set. Spearman’s rank correlation also evaluates the reliability of synthetic images for architecture search, comparing testing performances between models trained on proxy and real training sets. As illustrated in Tab. 8, D2M-generated images achieve the highest performance (88.8%) and a strong rank correlation (0.80) compared to priors.

## 5 Conclusion and Limitations

In this work, we introduce an efficient framework (D2M), which distills information from large-scale training datasets into the parameters of a pre-trained generative model instead of synthetic images. Our generative model employs carefully designed matching modules for distillation to enhance re-distillation efficiency, scalability to high-resolution datasets, and cross-architecture generality. We conduct extensive experiments across various datasets to demonstrate the efficiency and effectiveness of D2M. However, D2M needs more GPU memory in IPC1 compared to data distillation methods (Fig. 3). In the future, we plan to apply a more efficient generative model to small IPCs and explore D2M’s potential for other downstream tasks like object detection and segmentation.

## References

1. Amer, H., Salamah, A.H., Sajedi, A., Yang, E.h.: High performance convolution using sparsity and patterns for inference in deep convolutional neural networks. arXiv preprint arXiv:2104.08314 (2021)
2. Belouadah, E., Popescu, A.: Scail: Classifier weights scaling for class incremental learning. In: Proceedings of the IEEE/CVF winter conference on applications of computer vision. pp. 1266–1275 (2020)
3. Brock, A., Donahue, J., Simonyan, K.: Large scale gan training for high fidelity natural image synthesis. In: International Conference on Learning Representations (2018)
4. Brown, T., Mann, B., Ryder, N., Subbiah, M., Kaplan, J.D., Dhariwal, P., Neelakantan, A., Shyam, P., Sastry, G., Askell, A., et al.: Language models are few-shot learners. *Advances in neural information processing systems* **33**, 1877–1901 (2020)
5. Cazenavette, G., Wang, T., Torralba, A., Efros, A.A., Zhu, J.Y.: Dataset distillation by matching training trajectories. In: Proceedings of the IEEE/CVF Conference on Computer Vision and Pattern Recognition. pp. 4750–4759 (2022)
6. Cazenavette, G., Wang, T., Torralba, A., Efros, A.A., Zhu, J.Y.: Generalizing dataset distillation via deep generative prior. In: Proceedings of the IEEE/CVF Conference on Computer Vision and Pattern Recognition. pp. 3739–3748 (2023)
7. Chen, D., Kerkouche, R., Fritz, M.: Private set generation with discriminative information. *Advances in Neural Information Processing Systems* **35**, 14678–14690 (2022)
8. Chen, L., Zhang, H., Xiao, J., Nie, L., Shao, J., Liu, W., Chua, T.S.: Sca-cnn: Spatial and channel-wise attention in convolutional networks for image captioning. In: Proceedings of the IEEE conference on computer vision and pattern recognition. pp. 5659–5667 (2017)
9. Chen, X., Duan, Y., Houthoofd, R., Schulman, J., Sutskever, I., Abbeel, P.: Infogan: Interpretable representation learning by information maximizing generative adversarial nets. *Advances in neural information processing systems* **29** (2016)
10. Chen, X., Yang, Y., Wang, Z., Mirzasoleiman, B.: Data distillation can be like vodka: Distilling more times for better quality. arXiv preprint arXiv:2310.06982 (2023)
11. Child, R.: Very deep vaes generalize autoregressive models and can outperform them on images. In: International Conference on Learning Representations (2021)
12. Ciftci, U.A., Yuksek, G., Demir, I.: My face my choice: Privacy enhancing deep-fakes for social media anonymization. In: Proceedings of the IEEE/CVF Winter Conference on Applications of Computer Vision. pp. 1369–1379 (2023)
13. Cui, J., Wang, R., Si, S., Hsieh, C.J.: Scaling up dataset distillation to imagenet-1k with constant memory. In: International Conference on Machine Learning. pp. 6565–6590. PMLR (2023)
14. Deng, J., Dong, W., Socher, R., Li, L.J., Li, K., Fei-Fei, L.: Imagenet: A large-scale hierarchical image database. In: 2009 IEEE conference on computer vision and pattern recognition. pp. 248–255. Ieee (2009)
15. Dong, T., Zhao, B., Lyu, L.: Privacy for free: How does dataset condensation help privacy? In: International Conference on Machine Learning. pp. 5378–5396. PMLR (2022)
16. Dosovitskiy, A., Beyer, L., Kolesnikov, A., Weissenborn, D., Zhai, X., Unterthiner, T., Dehghani, M., Minderer, M., Heigold, G., Gelly, S., et al.: An image is worth 16x16 words: Transformers for image recognition at scale. arXiv preprint arXiv:2010.11929 (2020)

17. Du, J., Jiang, Y., Tan, V.Y., Zhou, J.T., Li, H.: Minimizing the accumulated trajectory error to improve dataset distillation. In: Proceedings of the IEEE/CVF Conference on Computer Vision and Pattern Recognition. pp. 3749–3758 (2023)
18. Du, J., Shi, Q., Zhou, J.T.: Sequential subset matching for dataset distillation. *Advances in Neural Information Processing Systems* **36** (2024)
19. Furlanello, T., Lipton, Z., Tschannen, M., Itti, L., Anandkumar, A.: Born again neural networks. In: International Conference on Machine Learning. pp. 1607–1616. PMLR (2018)
20. Gidaris, S., Komodakis, N.: Dynamic few-shot visual learning without forgetting. In: Proceedings of the IEEE conference on computer vision and pattern recognition. pp. 4367–4375 (2018)
21. Goodfellow, I., Pouget-Abadie, J., Mirza, M., Xu, B., Warde-Farley, D., Ozair, S., Courville, A., Bengio, Y.: Generative adversarial nets. *Advances in neural information processing systems* **27** (2014)
22. Gu, J., Wang, K., Jiang, W., You, Y.: Summarizing stream data for memory-restricted online continual learning. In: Proceedings of the AAAI Conference on Artificial Intelligence (AAAI) (2024)
23. Guo, Z., Wang, K., Cazenavette, G., LI, H., Zhang, K., You, Y.: Towards lossless dataset distillation via difficulty-aligned trajectory matching. In: The Twelfth International Conference on Learning Representations (2024), <https://openreview.net/forum?id=rTBL80hdhH>
24. He, J., Shi, W., Chen, K., Fu, L., Dong, C.: Gcfsr: a generative and controllable face super resolution method without facial and gan priors. In: Proceedings of the IEEE/CVF Conference on Computer Vision and Pattern Recognition. pp. 1889–1898 (2022)
25. He, K., Zhang, X., Ren, S., Sun, J.: Delving deep into rectifiers: Surpassing human-level performance on imagenet classification. In: Proceedings of the IEEE international conference on computer vision. pp. 1026–1034 (2015)
26. He, K., Zhang, X., Ren, S., Sun, J.: Deep residual learning for image recognition. In: Proceedings of the IEEE conference on computer vision and pattern recognition. pp. 770–778 (2016)
27. He, Y., Xiao, L., Zhou, T.J.: You Only Condense Once: Two rules for pruning condensed datasets. In: Proceedings of the Advances in Neural Information Processing Systems (NeurIPS) (2023)
28. Hinton, G., Vinyals, O., Dean, J.: Distilling the knowledge in a neural network. arXiv preprint arXiv:1503.02531 (2015)
29. Ho, J., Ermon, S.: Generative adversarial imitation learning. *Advances in neural information processing systems* **29** (2016)
30. Howard, J.: Imagenette: A smaller subset of 10 easily classified classes from imagenet, and a little more french (2019)
31. Huang, G., Liu, Z., Van Der Maaten, L., Weinberger, K.Q.: Densely connected convolutional networks. In: Proceedings of the IEEE conference on computer vision and pattern recognition. pp. 4700–4708 (2017)
32. Jin, Y., Wang, J., Lin, D.: Multi-level logit distillation. In: Proceedings of the IEEE/CVF Conference on Computer Vision and Pattern Recognition. pp. 24276–24285 (2023)
33. Kenton, J.D.M.W.C., Toutanova, L.K.: Bert: Pre-training of deep bidirectional transformers for language understanding. In: Proceedings of NAACL-HLT. pp. 4171–4186 (2019)

34. Khaki, S., Luo, W.: Cfdp: Common frequency domain pruning. In: Proceedings of the IEEE/CVF Conference on Computer Vision and Pattern Recognition. pp. 4714–4723 (2023)
35. Khaki, S., Plataniotis, K.N.: The need for speed: Pruning transformers with one recipe. arXiv preprint arXiv:2403.17921 (2024)
36. Khaki, S., Sajedi, A., Wang, K., Liu, L.Z., Lawryshyn, Y.A., Plataniotis, K.N.: Atom: Attention mixer for efficient dataset distillation. In: Proceedings of the IEEE/CVF Conference on Computer Vision and Pattern Recognition. pp. 7692–7702 (2024)
37. Kim, J.H., Kim, J., Oh, S.J., Yun, S., Song, H., Jeong, J., Ha, J.W., Song, H.O.: Dataset condensation via efficient synthetic-data parameterization. In: International Conference on Machine Learning. pp. 11102–11118. PMLR (2022)
38. Krizhevsky, A., Hinton, G., et al.: Learning multiple layers of features from tiny images (2009)
39. Krizhevsky, A., Sutskever, I., Hinton, G.E.: Imagenet classification with deep convolutional neural networks. *Communications of the ACM* **60**(6), 84–90 (2017)
40. Le, Y., Yang, X.: Tiny imagenet visual recognition challenge. *CS 231N* **7**(7), 3 (2015)
41. Ledig, C., Theis, L., Huszár, F., Caballero, J., Cunningham, A., Acosta, A., Aitken, A., Tejani, A., Totz, J., Wang, Z., et al.: Photo-realistic single image super-resolution using a generative adversarial network. In: Proceedings of the IEEE conference on computer vision and pattern recognition. pp. 4681–4690 (2017)
42. Lee, C.H., Liu, Z., Wu, L., Luo, P.: Maskgan: Towards diverse and interactive facial image manipulation. In: Proceedings of the IEEE/CVF Conference on Computer Vision and Pattern Recognition. pp. 5549–5558 (2020)
43. Lee, S., Chun, S., Jung, S., Yun, S., Yoon, S.: Dataset condensation with contrastive signals. In: International Conference on Machine Learning. pp. 12352–12364. PMLR (2022)
44. Li, C., Lin, M., Ding, Z., Lin, N., Zhuang, Y., Huang, Y., Ding, X., Cao, L.: Knowledge condensation distillation. In: European Conference on Computer Vision. pp. 19–35. Springer (2022)
45. Li, H., Kadav, A., Durdanovic, I., Samet, H., Graf, H.P.: Pruning filters for efficient convnets. In: International Conference on Learning Representations (2017)
46. Li, J., Liang, X., Wei, Y., Xu, T., Feng, J., Yan, S.: Perceptual generative adversarial networks for small object detection. In: Proceedings of the IEEE conference on computer vision and pattern recognition. pp. 1222–1230 (2017)
47. Liu, L., Muelly, M., Deng, J., Pfister, T., Li, L.J.: Generative modeling for small-data object detection. In: Proceedings of the IEEE/CVF International Conference on Computer Vision. pp. 6073–6081 (2019)
48. Liu, P., Yu, X., Zhou, J.T.: Meta knowledge condensation for federated learning. In: The Eleventh International Conference on Learning Representations (2022)
49. Liu, S., Wang, K., Yang, X., Ye, J., Wang, X.: Dataset distillation via factorization. *Advances in Neural Information Processing Systems* **35**, 1100–1113 (2022)
50. Liu, S., Ye, J., Yu, R., Wang, X.: Slimmable dataset condensation. In: Proceedings of the IEEE/CVF Conference on Computer Vision and Pattern Recognition. pp. 3759–3768 (2023)
51. Liu, Y., Gu, J., Wang, K., Zhu, Z., Jiang, W., You, Y.: Dream: Efficient dataset distillation by representative matching. arXiv preprint arXiv:2302.14416 (2023)
52. Loo, N., Hasani, R., Amini, A., Rus, D.: Efficient dataset distillation using random feature approximation. *Advances in Neural Information Processing Systems* **35**, 13877–13891 (2022)

53. Loo, N., Hasani, R., Lechner, M., Amini, A., Rus, D.: Understanding reconstruction attacks with the neural tangent kernel and dataset distillation (2023)
54. Ma, C., Huang, J.B., Yang, X., Yang, M.H.: Hierarchical convolutional features for visual tracking. In: Proceedings of the IEEE international conference on computer vision. pp. 3074–3082 (2015)
55. Van der Maaten, L., Hinton, G.: Visualizing data using t-sne. *Journal of machine learning research* **9**(11) (2008)
56. Mirza, M., Osindero, S.: Conditional generative adversarial nets. arXiv preprint arXiv:1411.1784 (2014)
57. Molchanov, P., Tyree, S., Karras, T., Aila, T., Kautz, J.: Pruning convolutional neural networks for resource efficient inference. In: International Conference on Learning Representations (2019)
58. Nguyen, T., Chen, Z., Lee, J.: Dataset meta-learning from kernel-ridge regression. In: International Conference on Learning Representations (2021), <https://openreview.net/forum?id=1-PrrQrK0QR>
59. Nguyen, T., Novak, R., Xiao, L., Lee, J.: Dataset distillation with infinitely wide convolutional networks. *Advances in Neural Information Processing Systems* **34**, 5186–5198 (2021)
60. Park, W., Kim, D., Lu, Y., Cho, M.: Relational knowledge distillation. In: Proceedings of the IEEE/CVF conference on computer vision and pattern recognition. pp. 3967–3976 (2019)
61. Rebuffi, S.A., Kolesnikov, A., Sperl, G., Lampert, C.H.: icarl: Incremental classifier and representation learning. In: Proceedings of the IEEE conference on Computer Vision and Pattern Recognition. pp. 2001–2010 (2017)
62. Romero, A., Ballas, N., Kahou, S.E., Chassang, A., Gatta, C., Bengio, Y.: Fitnets: Hints for thin deep nets. arXiv preprint arXiv:1412.6550 (2014)
63. Saito, K., Watanabe, K., Ushiku, Y., Harada, T.: Maximum classifier discrepancy for unsupervised domain adaptation. In: Proceedings of the IEEE conference on computer vision and pattern recognition. pp. 3723–3732 (2018)
64. Sajedi, A., Khaki, S., Amjadi, E., Liu, L.Z., Lawryshyn, Y.A., Plataniotis, K.N.: Datadam: Efficient dataset distillation with attention matching. In: Proceedings of the IEEE/CVF International Conference on Computer Vision. pp. 17097–17107 (2023)
65. Sajedi, A., Khaki, S., Lawryshyn, Y.A., Plataniotis, K.N.: Probmcl: Simple probabilistic contrastive learning for multi-label visual classification. In: ICASSP 2024-2024 IEEE International Conference on Acoustics, Speech and Signal Processing (ICASSP). pp. 5115–5119. IEEE (2024)
66. Sajedi, A., Khaki, S., Plataniotis, K.N., Hosseini, M.S.: End-to-end supervised multilabel contrastive learning. arXiv preprint arXiv:2307.03967 (2023)
67. Sajedi, A., Lawryshyn, Y.A., Plataniotis, K.N.: Subclass knowledge distillation with known subclass labels. In: 2022 IEEE 14th Image, Video, and Multidimensional Signal Processing Workshop (IVMSP). pp. 1–5. IEEE (2022)
68. Sajedi, A., Plataniotis, K.N.: On the efficiency of subclass knowledge distillation in classification tasks. arXiv preprint arXiv:2109.05587 (2021)
69. Sauer, A., Schwarz, K., Geiger, A.: Stylegan-xl: Scaling stylegan to large diverse datasets. In: ACM SIGGRAPH 2022 conference proceedings. pp. 1–10 (2022)
70. Sener, O., Savarese, S.: Active learning for convolutional neural networks: A core-set approach. In: International Conference on Learning Representations (2018)
71. Simonyan, K., Zisserman, A.: Very deep convolutional networks for large-scale image recognition. arXiv preprint arXiv:1409.1556 (2014)

72. Sohn, K., Lee, H., Yan, X.: Learning structured output representation using deep conditional generative models. *Advances in neural information processing systems* **28** (2015)
73. Such, F.P., Rawal, A., Lehman, J., Stanley, K., Clune, J.: Generative teaching networks: Accelerating neural architecture search by learning to generate synthetic training data. In: *International Conference on Machine Learning*. pp. 9206–9216. PMLR (2020)
74. Tan, M., Le, Q.: Efficientnet: Rethinking model scaling for convolutional neural networks. In: *International conference on machine learning*. pp. 6105–6114. PMLR (2019)
75. Toneva, M., Sordoni, A., des Combes, R.T., Trischler, A., Bengio, Y., Gordon, G.J.: An empirical study of example forgetting during deep neural network learning. In: *International Conference on Learning Representations* (2019)
76. Tschandl, P., Rosendahl, C., Kittler, H.: The ham10000 dataset, a large collection of multi-source dermatoscopic images of common pigmented skin lesions. *Scientific data* **5**(1), 1–9 (2018)
77. Ulyanov, D., Vedaldi, A., Lempitsky, V.: Instance normalization: The missing ingredient for fast stylization. *arXiv preprint arXiv:1607.08022* (2016)
78. Wang, K., Gu, J., Zhou, D., Zhu, Z., Jiang, W., You, Y.: Dim: Distilling dataset into generative model. *arXiv preprint arXiv:2303.04707* (2023)
79. Wang, K., Zhao, B., Peng, X., Zhu, Z., Yang, S., Wang, S., Huang, G., Bilén, H., Wang, X., You, Y.: Cafe: Learning to condense dataset by aligning features. In: *Proceedings of the IEEE/CVF Conference on Computer Vision and Pattern Recognition*. pp. 12196–12205 (2022)
80. Wang, T.C., Liu, M.Y., Zhu, J.Y., Tao, A., Kautz, J., Catanzaro, B.: High-resolution image synthesis and semantic manipulation with conditional gans. In: *Proceedings of the IEEE conference on computer vision and pattern recognition*. pp. 8798–8807 (2018)
81. Wang, T., Zhu, J.Y., Torralba, A., Efros, A.A.: Dataset distillation. *arXiv preprint arXiv:1811.10959* (2018)
82. Wang, Y.R., Khaki, S., Zheng, W., Hosseini, M.S., Plataniotis, K.N.: Conetv2: Efficient auto-channel size optimization for cnns. In: *2021 20th IEEE International Conference on Machine Learning and Applications (ICMLA)*. pp. 998–1003 (2021). <https://doi.org/10.1109/ICMLA52953.2021.00164>
83. Wu, J., Leng, C., Wang, Y., Hu, Q., Cheng, J.: Quantized convolutional neural networks for mobile devices. In: *Proceedings of the IEEE conference on computer vision and pattern recognition*. pp. 4820–4828 (2016)
84. Xiong, Y., Wang, R., Cheng, M., Yu, F., Hsieh, C.J.: Feddm: Iterative distribution matching for communication-efficient federated learning. In: *Proceedings of the IEEE/CVF Conference on Computer Vision and Pattern Recognition*. pp. 16323–16332 (2023)
85. Yang, E., Shen, L., Wang, Z., Liu, T., Guo, G.: An efficient dataset condensation plugin and its application to continual learning. *Advances in Neural Information Processing Systems* **36** (2024)
86. Yang, J., Shi, R., Wei, D., Liu, Z., Zhao, L., Ke, B., Pfister, H., Ni, B.: Medmnist v2—a large-scale lightweight benchmark for 2d and 3d biomedical image classification. *Scientific Data* **10**(1), 41 (2023)
87. Yin, Z., Xing, E., Shen, Z.: Squeeze, recover and relabel: Dataset condensation at imagenet scale from a new perspective. In: *Proceedings of the Advances in Neural Information Processing Systems (NeurIPS)* (2023)

88. Yuan, L., Tay, F.E., Li, G., Wang, T., Feng, J.: Revisiting knowledge distillation via label smoothing regularization. In: Proceedings of the IEEE/CVF Conference on Computer Vision and Pattern Recognition. pp. 3903–3911 (2020)
89. Zagoruyko, S., Komodakis, N.: Paying more attention to attention: Improving the performance of convolutional neural networks via attention transfer. In: International Conference on Learning Representations (2016)
90. Zhang, L., Zhang, J., Lei, B., Mukherjee, S., Pan, X., Zhao, B., Ding, C., Li, Y., Xu, D.: Accelerating dataset distillation via model augmentation. In: Proceedings of the IEEE/CVF Conference on Computer Vision and Pattern Recognition. pp. 11950–11959 (2023)
91. Zhao, B., Bilen, H.: Dataset condensation with differentiable siamese augmentation. In: International Conference on Machine Learning. pp. 12674–12685. PMLR (2021)
92. Zhao, B., Bilen, H.: Synthesizing informative training samples with gan. In: NeurIPS 2022 Workshop on Synthetic Data for Empowering ML Research (2022)
93. Zhao, B., Bilen, H.: Dataset condensation with distribution matching. In: Proceedings of the IEEE/CVF Winter Conference on Applications of Computer Vision. pp. 6514–6523 (2023)
94. Zhao, B., Mopuri, K.R., Bilen, H.: Dataset condensation with gradient matching. In: Ninth International Conference on Learning Representations 2021 (2021)
95. Zhao, G., Li, G., Qin, Y., Yu, Y.: Improved distribution matching for dataset condensation. In: Proceedings of the IEEE/CVF Conference on Computer Vision and Pattern Recognition. pp. 7856–7865 (2023)
96. Zhou, D., Wang, K., Gu, J., Peng, X., Lian, D., Zhang, Y., You, Y., Feng, J.: Dataset quantization. In: Proceedings of the IEEE/CVF International Conference on Computer Vision. pp. 17205–17216 (2023)
97. Zhou, Y., Nezhadarya, E., Ba, J.: Dataset distillation using neural feature regression. In: Advances in Neural Information Processing Systems (2022)
98. Zhu, J.Y., Park, T., Isola, P., Efros, A.A.: Unpaired image-to-image translation using cycle-consistent adversarial networks. In: Proceedings of the IEEE international conference on computer vision. pp. 2223–2232 (2017)

## A Supplementary Materials

Here we include additional details of our experiments, evaluation framework, and further results.

## B Clarifying the Evaluation Framework

Early on in this project, we struggled to find a fair way to evaluate our distillation method against other image distillation methods. In previous iterations of this work, we proposed our setting as a fixed IPC comparison. Under this setting, we generate a fixed number of images to compare with other IPC-based works such as CAFE [79], DataDAM [64], MTT [5], etc. Ultimately we evolved this setting into our current version at ECCV. In our current setting, and previous iterations, we generate a fixed number of images per class, however there are multiple ways to *fix* the number of images per class. One could match the storage costs, or in our case, the latency. We measure the time it takes to train a downstream network on IPC images, this creates a fixed time cost per network, and per configuration. We can use this time cost to distribute the number of images we produce against the time taken to train our downstream network. We note that this *still* retains a fixed number of images and that the raw amount of images is determined by the fixed time ratio per configuration. In previous iterations of our work, we simply refer to this setting as *fixed* IPC, which in turn is correct, but we feel adding this message is valuable for the community to discuss and understand how our definition of *fixed IPC* may differ from previous works, while still retaining a fair comparison. In conclusion our evaluation protocols match the evaluation time constraints of training a target downstream model on IPC images, however we divide this time between generation of a fixed number of images (determined by the time ratio) and the actual training. This protocol still differs from previous works such as DiM [78], as we are not generating on the fly – rather allocated a fixed time block to generate a fixed number of image such that the total time remains equivalent.

## C Implementation Details

### C.1 Datasets

We conduct a comprehensive series of experiments involving a variety of datasets, including CIFAR10/100 [38], Tiny ImageNet [40], ImageNet-1K [14], and specific subsets of ImageNet-1K, namely ImageNette [30], ImageWoof [30], and ImageSquawk [5]. The CIFAR dataset, widely recognized in the field of low-resolution computer vision, comprises images of common objects rendered in  $32 \times 32$  pixels. This dataset is divided into two parts: CIFAR10, containing 10 broad categories, and CIFAR100, featuring 100 more detailed categories. Each part consists of 50,000 training images and 10,000 for testing. The CIFAR10 dataset classifies images into distinct categories such as "airplane", "car", "bird",

**Table 9:** Statistical properties of the datasets employed in the study.

Training Dataset	# of Classes	# of Images per class	Resolution
CIFAR-10 [38]	10	5000	32×32
CIFAR-100 [38]	100	500	32×32
Tiny ImageNet [40]	200	500	64×64
ImageNet-1K (128 × 128) [14]	1000	≈ 1200	64×64
ImageNet-1K Subsets (256×256) [5, 6]	10	≈ 1000-1200	128×128
DermaMNIST [86]	7	≈ 1400	256×256

"cat", "deer", "dog", "frog", "horse", "ship", and "truck". The Tiny ImageNet dataset is derived from the larger ImageNet-1K and includes 200 classes, with 100,000 training images and 10,000 testing images, all downsized to 64×64 pixels. In contrast, the more extensive ImageNet-1K dataset encompasses 1,000 categories, boasting over 1.2 million training images and 50,000 testing images. To align with the specifications of Tiny ImageNet, we resized the ImageNet-1K images to 64×64 pixels, following established procedures outlined in [64, 93, 97]. The Tiny ImageNet and ImageNet-1K datasets present a higher level of complexity compared to CIFAR-10/100 due to their broader class range and increased image resolution. Our study goes further by incorporating high-resolution images, specifically the 128×128 pixel versions of ImageNet-1K and its subsets. While previous dataset distillation studies [5, 6] focused on subsets categorized by themes such as birds, fruits, and cats, our research takes a more comprehensive approach by including several subsets like ImageNette (assorted items), ImageWoof (dog breeds), ImageSquawk (bird species), ImageFruit, and ImageMeow (cat species). This demonstrates the robustness of our method, D2M across a broad range of datasets.

It is worth noting that we have finally extended the application of D2M to higher resolutions, specifically 256×256 for the Image-Squawk dataset and medical imaging DermaMNIST [86]. The DermaMNIST makes use of the HAM10000 dataset [76], which is a comprehensive collection of dermatoscopic images depicting various common pigmented skin lesions. This dataset includes 10,015 dermatoscopic images classified into seven different diseases, posing a multi-class classification challenge. To facilitate model training and evaluation, we divided the images into training, validation, and test sets with a 7:1:2 ratio. An overview of the statistical characteristics of the datasets used in our study is presented in Table 9.

Additionally, in the supplementary materials, we conducted a comparative analysis between our methodology and GLaD [6], applying it to newly created high-resolution (128×128 pixel) 10-class subsets from ImageNet-1K. These high-resolution subsets were created based on the performance evaluation of a pre-trained ResNet-50 [26] model on ImageNet-1K, as detailed in [6]. Our experiments contained "ImageNet-A", which included the top 10 classes, followed by "ImageNet-B" with the next 10, and so forth, up to "ImageNet-E". For a

**Table 10:** Class listings for the ImageNet-1K [14] subsets.

Dataset	0	1	2	3	4	5	6	7	8	9
ImageNet1 [30]	Trench	English Springer	Cassette Player	Chainsaw	Church	French Horn	Garbage Truck	Gas Pump	Golf Ball	Parachute
ImageNet2 [30]	Australian Terrier	Border Terrier	Samoyed	Beagle	Shih-Tzu	English Foxhound	Rhodesian Ridgeback	Dingo	Golden Retriever	English Sheepdog
ImageNet3 [5]	Peacock	Flamingo	Mincow	Pelican	King Penguin	Bald Eagle	Toucan	Ostrich	Black Swan	Cockatoo
ImageNet4 [5]	Pineapple	Banana	Strawberry	Orange	Lemon	Pomegranate	Fig	Bell Pepper	Cucumber	Granny Smith Apple
ImageNet5 [5]	Tabby Cat	Bengal Cat	Persian Cat	Siamese Cat	Egyptian Cat	Lion	Tiger	Jaguar	Snow Leopard	Lyx
ImageNet6 [6]	Leopard	Prohin Monkey	Rhesus	Three-Toed Sloth	Cliff Dwelling	Yellow Lady's Slipper	Hamster	Gambusia	Orc	Lingpin
ImageNet7 [6]	Spoonbill	Website	Lorikeet	Hyena	Earthstar	Trolleybus	Echidna	Pomeranian	Odometer	Ruddy Turnstone
ImageNet8 [6]	Freight Car	Hummingbird	Fireboat	Disk Brake	Bee Eater	Rock Beauty	Lion	European Gallinule	Cabbage Butterfly	Goldfinch
ImageNet9 [6]	Ostrich	Samoyed	Snowbird	Brabanson Griffin	Chickadee	Sorrel	Admiral	Great Gray Owl	Hornbill	Ringlet
ImageNet10 [6]	Spindle	Toucan	Black Swan	King Penguin	Potter's Wheel	Photocopier	Screw	Tarantula	Scilloscope	Lycanid

comprehensive list of the ImageNet classes within each subset, please refer to Table 10.

## C.2 Implementations of Prior Works

To ensure a fair comparison with prior studies, including [5, 6, 13, 17, 58, 59, 64, 79, 91–96], we obtained publicly available distilled data corresponding to each standard method and maintained consistent experimental settings during the evaluation phase. Our experimental setup featured a ConvNet architecture, which consisted of three, four, or five layers depending on the image resolutions. We also applied the same preprocessing techniques across all methodologies. In cases where our results matched or fell below the findings reported in their original papers, we directly presented their default values.

Kernel-based approaches, such as Kernel Inducing Points (KIP) [58, 59] and FRePo [97], employ significantly larger neural networks compared to other baseline methods. Specifically, the original KIP uses a larger model with a width of 1024 for evaluation, as opposed to the 128 used by other approaches. KIP also incorporates an additional convolutional layer compared to other methods. In the case of FRePo, it utilizes a distinct model that doubles the number of filters when the feature map size is halved. Furthermore, FRePo employs batch normalization instead of instance normalization. We made diligent efforts to replicate previous methods that lacked experiments on specific datasets by following the provided author codes. However, for techniques that encountered scalability challenges with high-resolution datasets, we were unable to obtain relevant performance metrics.

## C.3 Hyperparameters

To ensure the reproducibility of our methodology, we have provided Table 11, which details all the hyperparameters employed in this study. For the baseline methods, we adhered to the default parameters specified by the authors in their respective papers. Uniform hyperparameter settings were maintained throughout all experiments unless otherwise noted. Specifically, we utilized an SGD optimizer with a learning rate of  $1e-6$  during the distillation stage and a learning rate of 0.01 when training neural network models during the evaluation phase. For low-resolution datasets, we implemented a 3-layer ConvNet architecture, while for medium- and high-resolution datasets, we adopted the recommendations outlined in [93], employing 4-layer and 5-layer ConvNet architectures, respectively.

**Table 11:** Hyperparameters Details used in the D2M framework.

Hyperparameters			Options/ Range	Value
Category	Parameter Name	Description		
Optimization	Learning Rate $\eta_S$ (generator)	Step size towards global/local minima	(0, 10.0]	$1.0e-6$
	Learning Rate $\eta_D$ (network)	Step size towards global/local minima	(0, 1.0]	0.01
	Optimizer (generator)	Updates synthetic set to approach global/local minima	Adam	betas: (0.5, 0.9)
	Optimizer (network)	Updates model to approach global/local minima	SGD with Momentum	Momentum: 0.9 Weight Decay: $5e-4$
	Scheduler (generator)	-	-	-
	Scheduler (network)	Decays the learning rate over epochs	StepLR	Decay rate: 0.5 Step size: 15.0
	Epoch Count $K$	Number of epochs for generator matching	[1, $\infty$ )	60
Loss Function	Task Balance $\lambda$	Regularization Multiplier	[0, $\infty$ )	100
	Temperature Value $T$	Temperature in KL Divergence	[0, $\infty$ )	4
DSA Augmentations	Color	Randomly adjust (jitter) the color components of an image	brightness saturation contrast	1.0 2.0 0.5
	Crop	Crops an image with padding	ratio crop pad	0.125
	Cutout	Randomly covers input with a square	cutout ratio	0.5
	Flip	Flips an image with probability p in range:	(0, 1.0]	0.5
	Scale	Shifts pixels either column-wise or row-wise	scaling ratio	1.2
	Rotate	Rotates image by certain angle	$0^\circ - 360^\circ$	$[-15^\circ, +15^\circ]$
Encoder Parameters	Conv Layer Weights	The weights of convolutional layers	$\mathbb{R}$ bounded by kernel size	Uniform Distribution
	Activation Function	The non-linear function at the end of each layer	-	ReLU
	Normalization Layer	Type of normalization layer used after convolutional blocks	-	InstanceNorm
	Default Generator	Type of Generator used to produce synthetic distilled images	-	BigGan

**Table 12:** The performance comparison (%) for DREAM as a plug-and-play method with D2M.

Dataset	IPC	DREAM	D2M	DREAM + D2M
CIFAR-10	10	68.6 $\pm$ 0.5	67.8 $\pm$ 0.5	<b>69.5<math>\pm</math>0.3</b>
	50	74.6 $\pm$ 0.4	74.4 $\pm$ 0.4	<b>74.9<math>\pm</math>0.5</b>

Across all experiments, a mini-batch size of 128 real images was used for training over 60 epochs. We consistently applied a set of differentiable augmentations [91] during both the distillation and evaluation phases.

## D Additional Results and Further Analysis

### D.1 Comparison to More Baselines

**Comparison to IT-GAN [92].** Similar to GLaD [6], IT-GAN generates synthetic datasets in a generative model’s latent space. This is done by initially inverting the entire training set into the latent space and then fine-tuning the latent representations based on the distillation objective. IT-GAN does not reduce the number of synthesized images; they remain equal to the original dataset count. This differs from the typical aim of dataset distillation. For a fair comparison with D2M, we take a small subset (IPC10) of the IT-GAN-generated data (created with BigGAN [3]) as the "distilled dataset". We then evaluate this subset using ConvNet-3, comparing the results with D2M. IT-GAN achieved a 59.7% accuracy performance on CIFAR-10, a decrease of 8.1% compared to D2M. This finding suggests that our loss design effectively distills more informative knowledge into the generative model, aiding downstream classification tasks. It is also worth noting that, unlike D2M, both GLaD and IT-GAN require retraining of the distillation stage when there is a change in IPC or the distillation ratio.

**Comparison to DREAM [51].** In this section, we conduct a comparative analysis with a concurrent plug-and-play dataset distillation approach known as DREAM [51]. DREAM was introduced as a pre-processing technique for dataset distillation methods, serving as an informed selector when choosing images from the real training dataset for matching purposes. In the context of D2M, we have the opportunity to incorporate this pre-processing step to enhance the selection of images from the training data for our matching strategy. The authors of DREAM make a compelling argument that not all training data is equally beneficial for distilling knowledge from images. In our evaluation, we present the best performance achieved by DREAM when reproduced on our hardware, utilizing the optimal configuration as presented in their paper, as shown in Table 12. It is important to note that comparing DREAM to our baseline D2M in Tab. 1 of the main paper may not be fair. DREAM serves as a plug-and-play pre-processing step that complements other distillation algorithms, including DC [94], DM [93], and MTT [5]. Therefore, to provide a fair comparison, we have integrated DREAM pre-processing into our D2M method and reported the results in Table 12. We explicitly demonstrate that this augmented approach delivers superior performance, achieving the best results on CIFAR-10, particularly for IPC10 and 50, surpassing both our default D2M and the best results obtained by DREAM.

**Comparison to DiM [78].** DiM represents a concurrent approach in the realm of dataset distillation. In DiM, Wang *et al.* introduced a two-stage distillation process designed specifically for 10-class datasets. Initially, they train the generative model from scratch and subsequently incorporate a distillation loss to minimize differences in knowledge at the penultimate layer between real and synthetic images. In contrast, we propose a *single-stage* distillation applicable to *any* dataset, leveraging our novel matching modules to incorporate *attention maps* from intermediate layers and *soft output predictions* (i.e., dark knowledge).

**Evaluation of batch size  $B$  in D2M.** We evaluate the sensitivity of batch size  $B$  during the distillation stage by varying it within the range of 16 to 1024 on ConvNet-3. Notably, the default batch size  $B = 128$  yields the highest accuracy, as illustrated in Figure 6(b). Smaller batch sizes perform poorly due to their insufficient representativeness for feature matching and limited supervision from the original dataset in each iteration. In contrast, excessively large batch sizes, while providing more information, introduce optimization challenges and lead to a performance decrease. We notice that our generators remain completely stable during training. The only consideration here is the size of the optimization problem we are trying to solve. Specifically, increasing the batch size can complicate the tractability of the optimization problem and result in a more difficult optimization problem.

**Diffusion Model Analysis.** We extended our framework to the diffusion model (SD-XL) with LoRA fine-tuning on ImegeNette for IPC1. We achieved 52.1% which indicates the generalizability of D2M to diffusion models.

**Discriminator in D2M.** Including a discriminator in the distillation process is an interesting approach, but it increases the computational graph size,

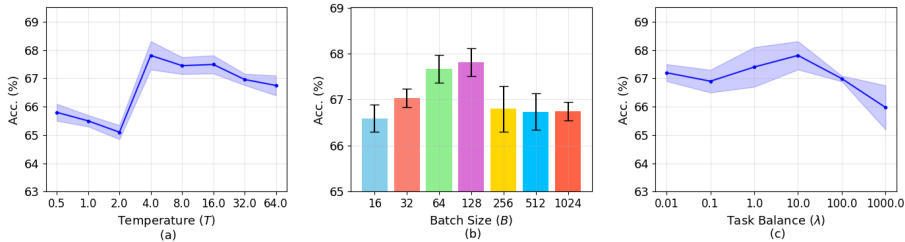


**Fig. 6:** The effect of (a) temperature, (b) batch size, and (c) task balance on the D2M’s performance for CIFAR10 with IPC10.

making it difficult to use in all our experiments. However, we conducted experiments on CIFAR-10 IPC1, comparing three configurations of our distillation loss: matching loss only (50.2%), matching loss with balanced discriminator loss (50.9%), and matching loss with large discriminator loss (43.8%). These results suggest that a strong discriminator can harm performance, while using discriminator loss as regularization improves results, likely due to reduced catastrophic forgetting. Thus, our matching loss is primarily responsible for making the images better suited for downstream training.

## D.2 Computational Cost Analysis

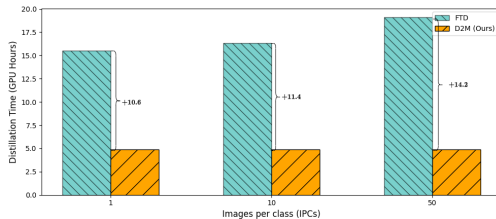
In the main paper, we conducted a thorough comparison of the re-distillation costs associated with D2M in comparison to other leading methods on the CIFAR-10 dataset. However, it is equally crucial to assess the distillation costs for each individual IPC setting. As there is always a trade-off between performance and computational demands, we used FTD [17] as a reference point. FTD is recognized as one of the top-tier methods in terms of performance for pixel-wise dataset distillation. We meticulously calculated the GPU hours required by both FTD and D2M during the distillation process on CIFAR-10 across IPC settings of 1, 10, and 50. As depicted in Figure 7, D2M’s GPU hour requirements for distillation remain consistent across different IPCs. This is because our proposed method distills knowledge from a real dataset into the parameters of the generative model rather than the raw pixels, and this process is independent of the number of images per class used for distillation. Conversely, in the case of FTD, computational costs increase as we elevate the IPC. It is important to mention that our method consistently outperforms FTD in terms of performance and computational costs, regardless of the IPC settings, as shown in Tab. 1 of the main paper and Figure 7, respectively.

The same trend holds for the number of learnable parameters. In the main paper (Fig. 3), we observed that on ImageNet-1K, D2M outperforms all pixel-wise dataset distillation methods in terms of the count of learnable parameters across most IPCs. To further evaluate this, we compared the number of learnable parameters trained on less complex datasets like CIFAR-100. As illustrated

**Table 13:** The GPU hours of the distillation time and the effort of image generation for different generative models on CIFAR-10.

Generative Model	Distillation Time (GPU hours)	Image Generation Time (ms)		
		IPC1	IPC10	IPC50
CGAN	2.1	1.46	5.08	20.58
BigGAN	4.9	5.42	15.50	59.92
StyleGAN-XL	8.9	26.84	125.33	518.53
CVAE	7.1	83.06	481.90	2203.48

in Figure 8, for small IPCs, pixel-wise distillation does exhibit some advantages over D2M. However, as we increase the number of images per class, D2M significantly outperforms pixel-wise distillation by a considerable margin, especially with IPC settings higher than 20. Therefore, we can conclude that D2M excels in computational efficiency and performance when working with complex and high-resolution datasets such as ImageNet-1K or Tiny ImageNet. In contrast, for simpler datasets like CIFAR-10/100, D2M remains at the forefront in terms of performance, regardless of the IPCs; however, it proves to be more computationally efficient in larger IPC settings.

**Fig. 7:** The GPU hours of the distillation time for FTD and D2M on CIFAR-10 with different IPCs.

**Computational costs of different generative models in D2M.** To enhance the computational efficiency of D2M when applied to less complex datasets, we conducted experiments using CIFAR-10 with various generative models, including conditional GAN (CGAN) [56], BigGAN [3], StyleGAN-XL [69], and CVAE [11, 72]. As shown in Table 13 and Figure 9, conditional GAN stood out for its remarkably short distillation time and a minimal number of learnable parameters, respectively. However, it is worth noting that this efficiency comes at the cost of a slight reduction in performance, as evidenced in Tab. 7 of the main paper. Consequently, we can conclude that when working with simple low-resolution datasets, opting for conditional GAN is a viable choice, even if it means sacrificing a small degree of accuracy compared to other generative models. However, in this work, we have selected BigGAN as the default gen-

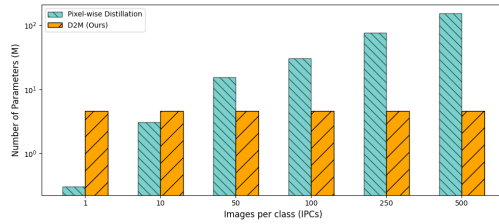


**Fig. 8:** Comparative analysis of the number of learnable parameters on  $32 \times 32$  resolution CIFAR-100 with different IPCs.

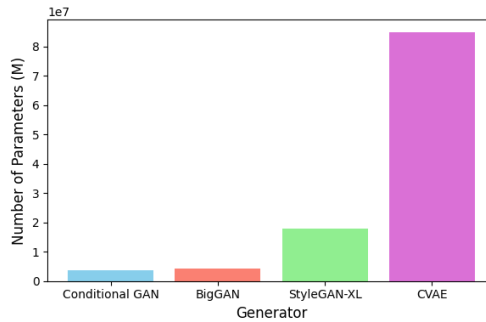


**Fig. 9:** Number of learnable parameters for different generative models on  $32 \times 32$  resolution CIFAR-10.

erative model across all experiments. This choice was made to strike a balance between performance and computational costs, particularly when dealing with extensive and high-resolution datasets. In such complex scenarios, D2M outperforms all other dataset distillation methods in terms of computational efficiency and performance, even in small IPCs.

Unlike the pixel-wise dataset distillation algorithms [5, 17, 51, 64, 79, 91, 94, 95, 97], D2M relies on generating training images in real-time during the evaluation stage. To understand the computational effort involved in this step, we conducted an experiment using the CIFAR-10 dataset to measure how long it takes to generate images with various generative models. The results, which you can find in Table 13, indicate that image generation typically takes just a few milliseconds when we use GAN-based generative models under different IPC settings. Importantly, the time spent on image generation is a small fraction of the total evaluation time, usually less than 0.6% when using BigGAN.

### D.3 More Details on Neural Architecture Search

Drawing on the studies in [91, 93, 94], we established a search domain containing 720 ConvNet configurations on the CIFAR-10 dataset. These models were evaluated using our distilled dataset, with an IPC of 50 serving as a proxy

dataset within the neural architecture search (NAS) paradigm. We initiated this process with a foundational ConvNet, forming a systematic grid that varies by depth  $D \in \{1, 2, 3, 4\}$ , width  $W \in \{32, 64, 128, 256\}$ , activation function  $A \in \{\text{Sigmoid}, \text{ReLu}, \text{LeakyReLu}\}$ , normalization technique  $N \in \{\text{None}, \text{Batch-Norm}, \text{LayerNorm}, \text{InstanceNorm}, \text{GroupNorm}\}$ , and pooling operation  $P \in \{\text{None}, \text{MaxPooling}, \text{AvgPooling}\}$ . These variants were then evaluated and hierarchically ordered based on their validation outcomes. In line with [64, 93], we randomly designated 10% of the CIFAR10 training samples as our validation subset, while the remainder formed the training set. The DSA augmentation [91] was applied across all proxy-set methods.

In Figure 10, we illustrate the rank correlation of performance between the proxy dataset—derived from various methodologies, including Random [61], DSA [91], DM [93], CAFE [79], DataDAM [64], D2M—and the full training dataset. We used Spearman’s rank correlation coefficient to analyze all 720 different architectural structures. Each point on the plot represents a unique architectural choice. The horizontal axis shows the test accuracy of models trained on the proxy dataset, while the vertical axis reflects the accuracy of models trained on the entire dataset. Our evaluation reveals that all methods are effective at generating reliable performance rankings for potential architectures. However, D2M stands out by having a larger cluster of points close to the straight line, indicating that it provides a more effective dataset for establishing dependable performance rankings of architectural choices. D2M achieves a remarkable correlation coefficient of 0.80, surpassing the benchmarks set by previous studies. The graph validates that our approach can yield a proxy dataset that obtains a more reliable performance ranking of candidate architectures.

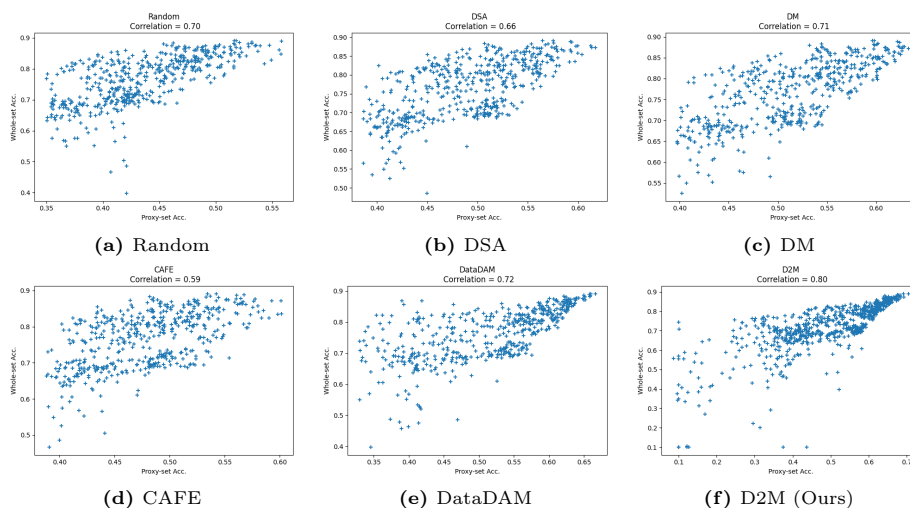


**Fig. 10:** Performance rank correlation between proxy-set and whole dataset training across all 720 architectures.

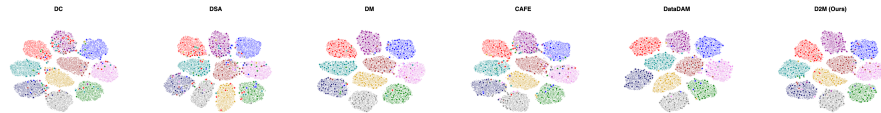


**Fig. 11:** Distributions of the synthetic images learned by six methods on the CIFAR10 dataset with IPC 50. The stars represent the synthetic data dispersed amongst the original dataset. The classes are as follows: plane, car, bird, cat, deer, dog, frog, horse, ship, truck.

## E Additional Visualizations

### E.1 Data Distribution

In order to assess the ability of our method to faithfully represent the distribution inherent in the original dataset, we employ t-SNE [55] for visualizing features extracted from both real and synthetically generated sets. These sets are produced by DC [94], DSA [91], DM [93], CAFE [79], DataDAM [64], and D2M, within the embedding space of the ResNet-18 architecture [26]. The visualizations were conducted using the CIFAR-10 dataset with an IPC50, a consistent choice across all methodologies.

As depicted in Figure 11, our approach, akin to DM and DataDAM, successfully preserves the dataset’s distribution, manifesting as a well-balanced dispersion across the entire dataset. Conversely, other methods such as DC, DSA, and CAFE exhibit noticeable biases towards certain cluster boundaries. In simpler terms, the t-SNE visualization validates that D2M maintains a significant degree of impartiality in accurately capturing the dataset’s distribution consistently across all categories. Preservation of dataset distributions holds paramount importance, particularly in domains like ethical machine learning, as methodologies that fail to capture data distribution can inadvertently introduce bias and discrimination. Our method’s capability to faithfully represent the data distribution renders it more suitable than alternative approaches, particularly in applications such as facial detection for privacy considerations [12].

### E.2 Visualization of the Generated Images

**Visualization of the images generated with D2M trained on different temperatures  $T$ .** This section examines the impact of temperature, denoted as  $T$ , on the generated synthetic images. As depicted in Fig. 4(a) in the main paper, it becomes apparent that a moderate temperature value enhances the influence of logit matching in KL-Divergence, resulting in better-distilled images suitable for classification and downstream tasks. We illustrate this qualitative effect by comparing its impact on CIFAR10 in Figure 18. We can clearly see that as we increase the temperature value from 0.5 to 8, there is a noticeable improvement in the localization and alignment of objects within the image, particularly within the ‘car’ and ‘bus’ classes. Meanwhile, when examining the image at  $T = 64$ ,

it appears that the quality and robustness of the image features have slightly diminished in comparison to the previous images. Nevertheless, it still retains a richer set of feature information compared to  $T = 1$ .

**Visualization of the images generated with D2M trained with different generative models.** In this section, we present visual comparisons of different backbone generative models used to produce our synthetic dataset. Specifically, we evaluate conditional GAN (Figure 19a), StyleGAN-XL (Figure 19b), and CVAE (Figure 19c), in comparison to BigGAN (as depicted in Figure 20 (a)). Upon qualitative analysis, we observe that the conditional GAN exhibits less distinct object localization compared to the other methods. This difference is particularly noticeable when examining the 'cat' and 'bird' classes. StyleGAN-XL stands out for producing high-quality images with rich colors and robust features across all categories. This is especially evident in the 'car,' 'airplane,' and 'ship' classes. Lastly, the CVAE also generates clear images; however, when compared to StyleGAN-XL, it tends to lose some relevant background information, notably in the 'airplane' class.

**Extended Visualizations.** We provide additional visualizations of the generated images for CIFAR-10 & CIFAR-100 in Figure 20, Tiny ImageNet & ImageNet-1K at resolution  $(64 \times 64)$  in Figure 21 and Figure 22-Figure 23, respectively. In the collection of figures presented in Figure 12, Figure 13, Figure 14, Figure 15, and Figure 16, we visually show how the higher resolution of  $256 \times 256$  pixels enhances object clarity and feature richness while preserving the properties of our matching algorithm. Notable improvements can be observed, such as the enhanced details of multiple heads in the 'eagle' class and the two-facing beaks in the 'toucan' class. In this resolution, we also provide the visualization of the generated images for the medical imaging DermaMNIST dataset in Figure 17. Furthermore, we provide ImageNet-1K at a resolution of  $128 \times 128$  in Figure 24, Figure 25, Figure 26, Figure 27, Figure 28, and all the associated subsets: ImageNette (Figure 29), ImageWoof (Figure 30), ImageSquawk (Figure 31), ImageFruit (Figure 32), ImageMeow (Figure 33), ImageNet-A (Figure 34), ImageNet-B (Figure 35), ImageNet-C (Figure 36), ImageNet-D (Figure 37), ImageNet-E (Figure 38).



**Fig. 12:** D2M-generated image visualization: ImageSquawk ( $256 \times 256$ ): (Top) 'ostrich' class, (Bottom) 'eagle' class.



**Fig. 13:** D2M-generated image visualization: ImageSquawk ( $256 \times 256$ ): (Top) 'peacock' class, (Bottom) 'macaw' class.



**Fig. 14:** D2M-generated image visualization: ImageSquawk ( $256 \times 256$ ): (Top) 'cockatoo' class, (Bottom) 'toucan' class.



**Fig. 15:** D2M-generated image visualization: ImageSquawk ( $256 \times 256$ ): (Top) 'black swan' class, (Bottom) 'flamingo' class.



**Fig. 16:** D2M-generated image visualization: ImageNet-1K ( $256 \times 256$ ): (Top) 'pelican' class, (Bottom) 'penguin' class

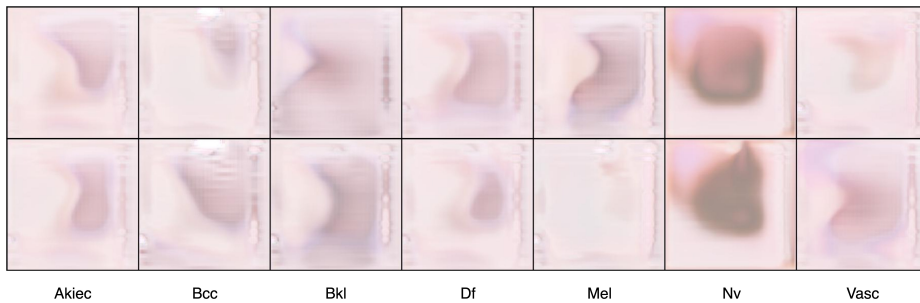


**Fig. 17:** D2M-generated image visualization: DermaMNIST ( $256 \times 256$ ) 7 classes. Class names under respective columns.

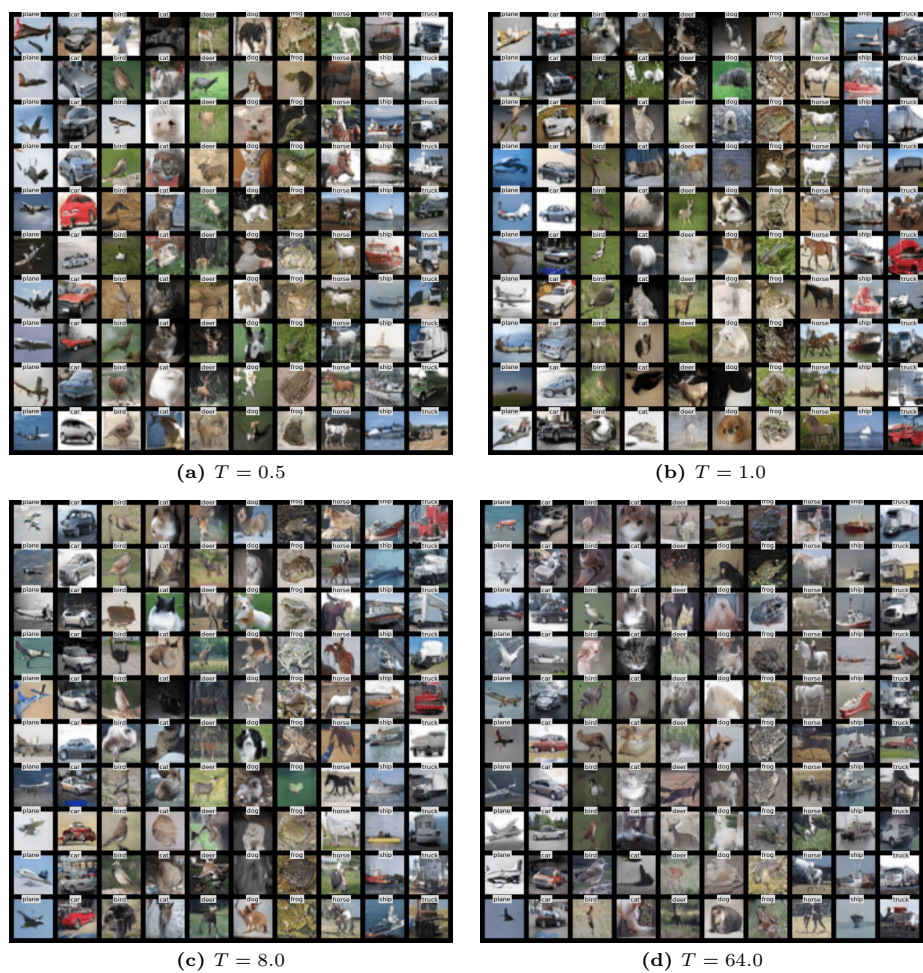


**Fig. 18:** D2M-generated image visualization (IPC10) for the CIFAR-10 dataset with different temperatures ( $T$ ) during distillation.

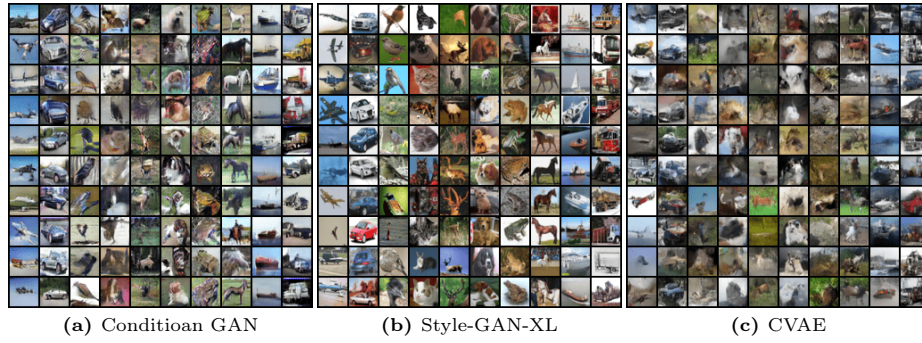


**Fig. 19:** D2M-generated image visualization (IPC10) for the CIFAR-10 dataset with different generative models.

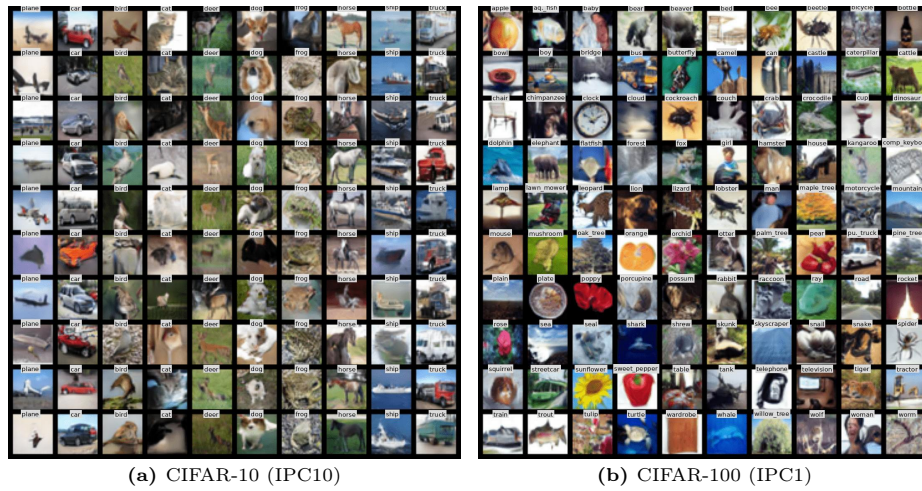


**Fig. 20:** D2M-generated image visualization: CIFAR datasets.

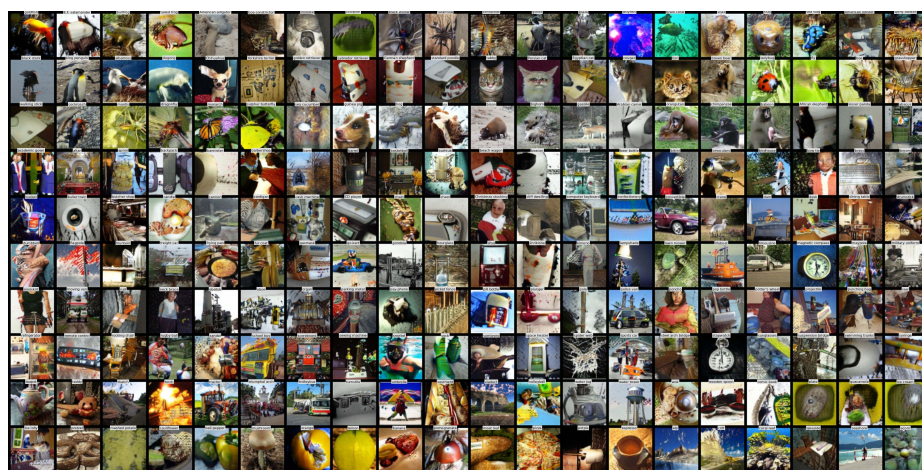


**Fig. 21:** D2M-generated image visualization: Tiny ImageNet ( $64 \times 64$ ) with IPC1.

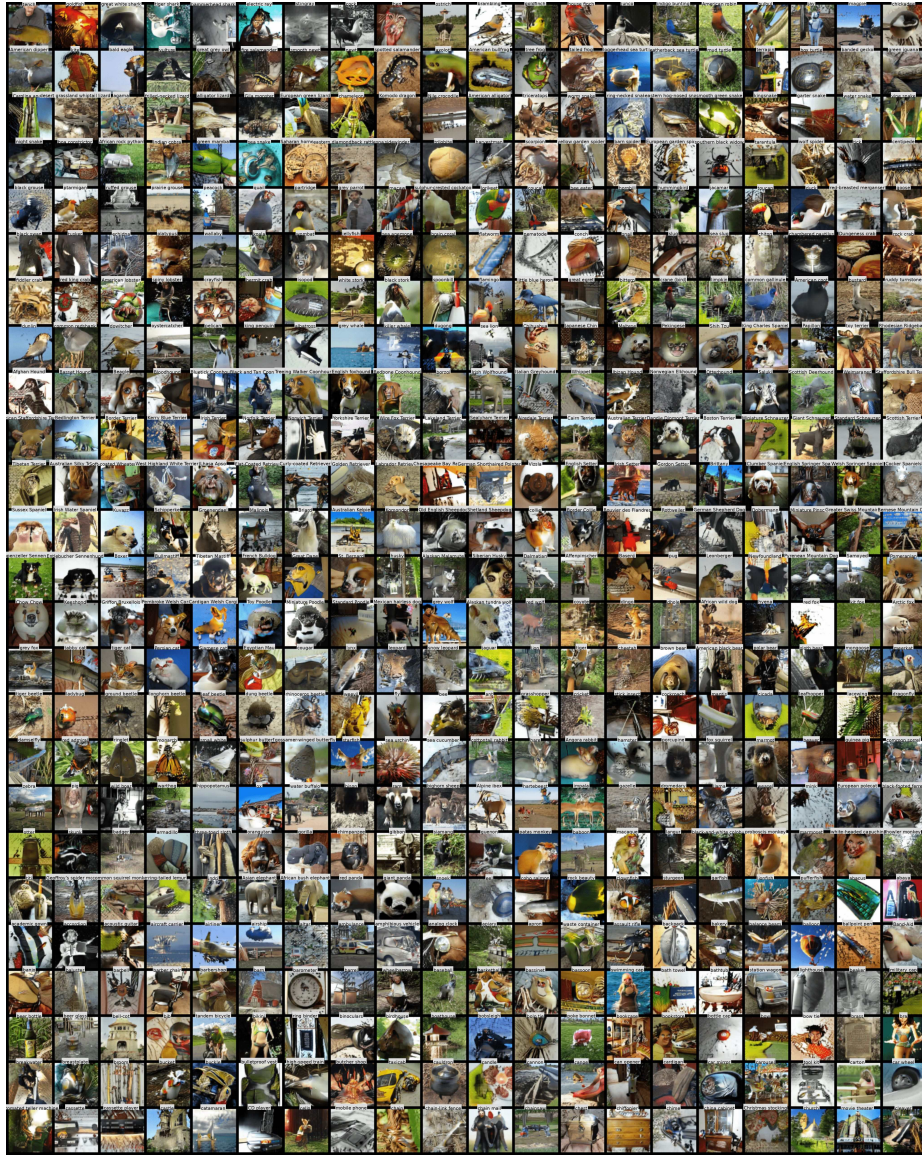


Fig. 22: D2M-generated image visualization: ImageNet-1K (64×64) Classes 0-500.



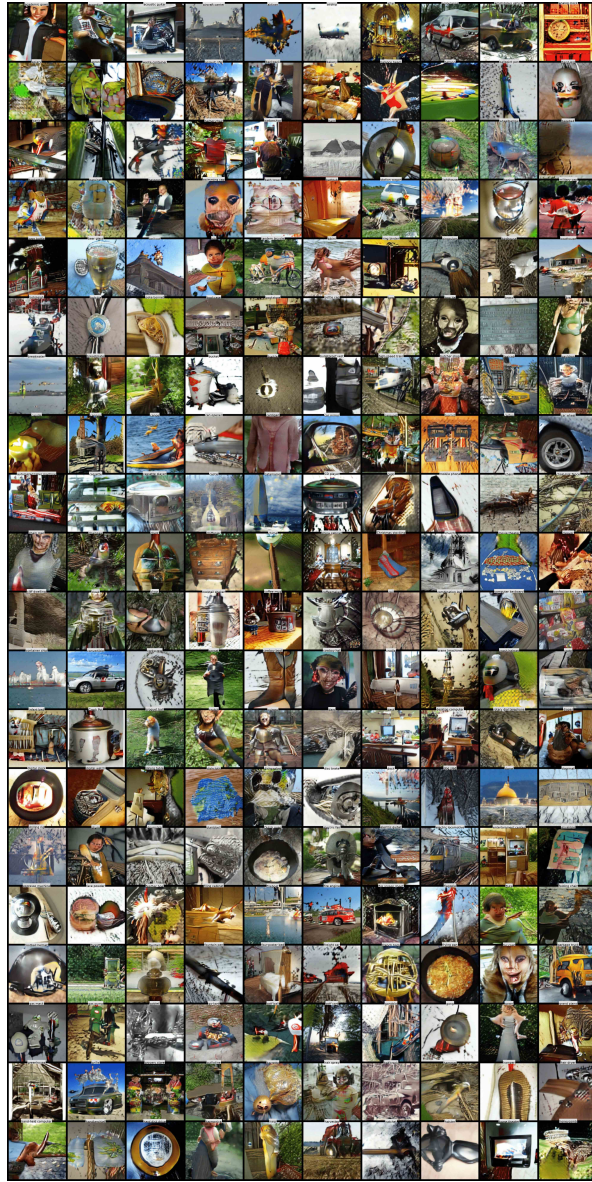
Fig. 23: D2M-generated image visualization: ImageNet-1K (64×64) Classes 500-1000.



Fig. 24: D2M-generated image visualization: ImageNet-1K ( $128 \times 128$ ) Classes 0-200.



**Fig. 25:** D2M-generated image visualization: ImageNet-1K ( $128 \times 128$ ) Classes 200-400.



**Fig. 26:** D2M-generated image visualization: ImageNet-1K ( $128 \times 128$ ) Classes 400-600.



**Fig. 27:** D2M-generated image visualization: ImageNet-1K ( $128 \times 128$ ) Classes 600-800.



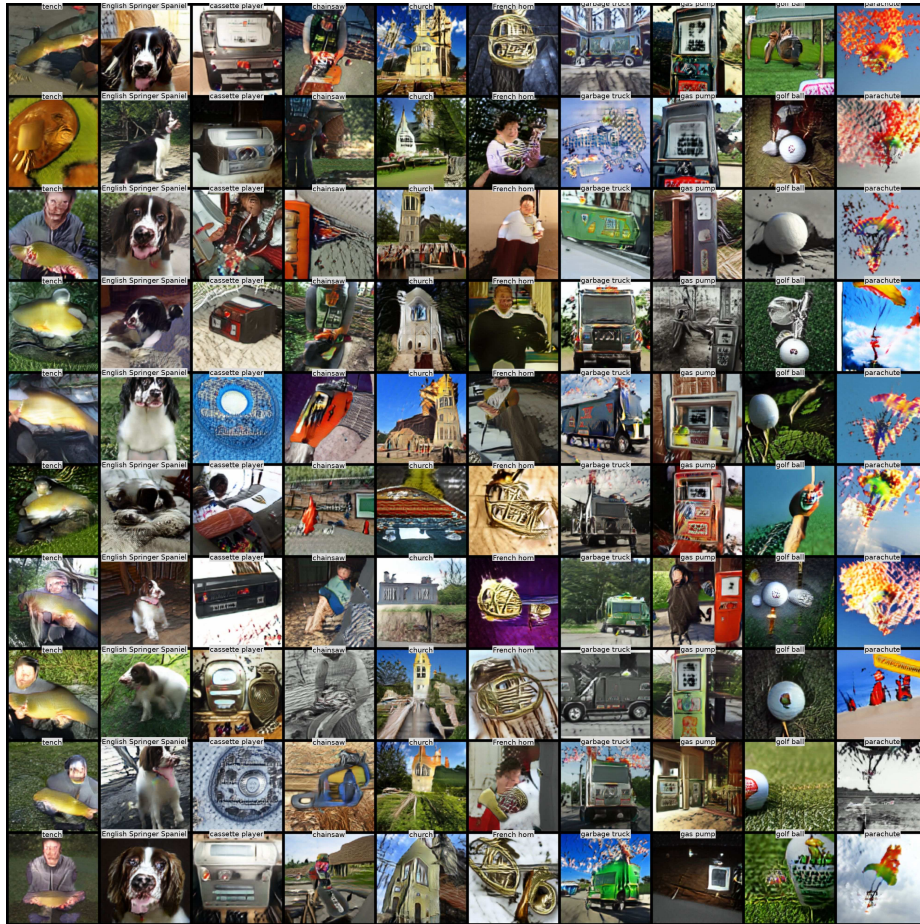


Fig. 29: D2M-generated image visualization: ImageNette Subset ( $128 \times 128$ ) with IPC1.



Fig. 30: D2M-generated image visualization: ImageWoof Subset ( $128 \times 128$ ) with IPC1.



**Fig. 31:** D2M-generated image visualization: ImageSquawk Subset ( $128 \times 128$ ) with IPC1.

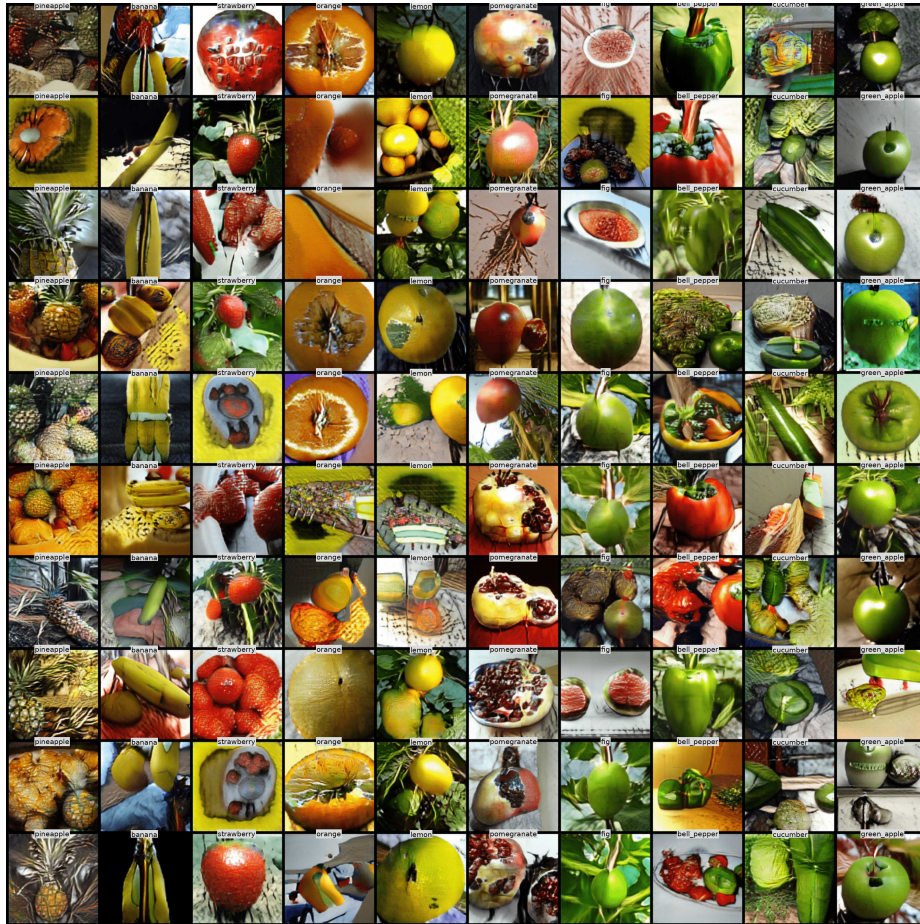
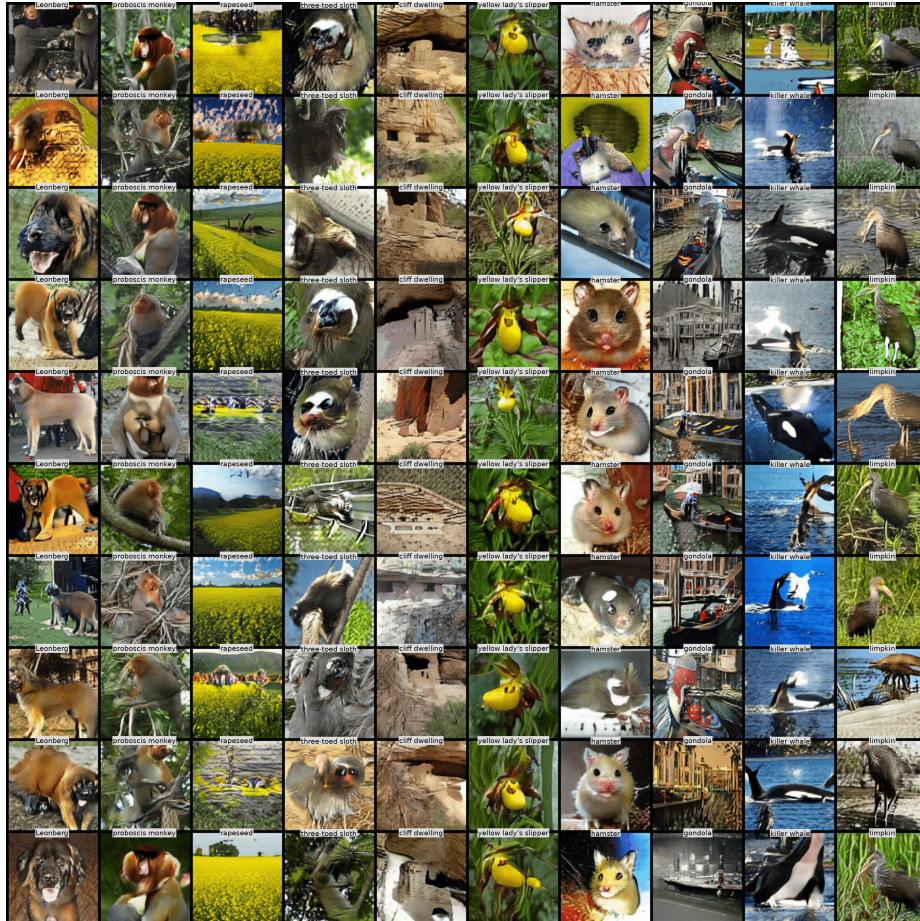


Fig. 32: D2M-generated image visualization: ImageFruit Subset ( $128 \times 128$ ) with IPC1.



**Fig. 33:** D2M-generated image visualization: ImageMeow Subset ( $128 \times 128$ ) with IPC1.



**Fig. 34:** D2M-generated image visualization: ImageNet-A Subset ( $128 \times 128$ ) with IPC1.

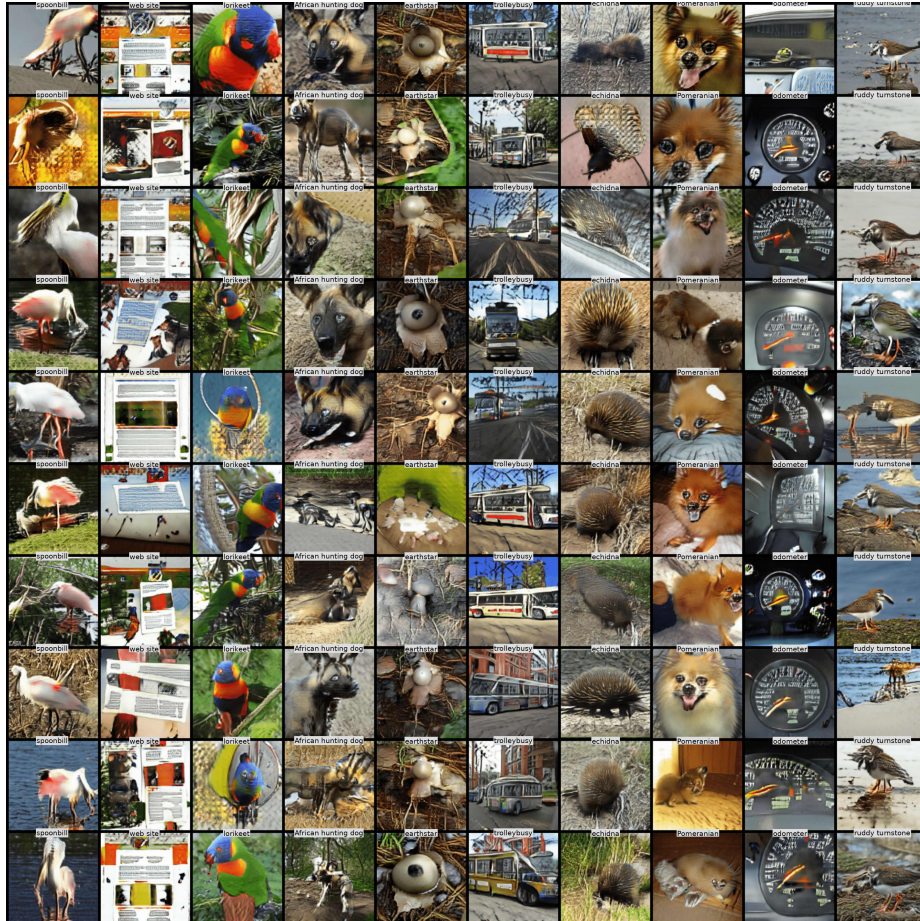


**Fig. 35:** D2M-generated image visualization: ImageNet-B Subset ( $128 \times 128$ ) with IPC1.



**Fig. 36:** D2M-generated image visualization: ImageNet-C Subset ( $128 \times 128$ ) with IPC1.

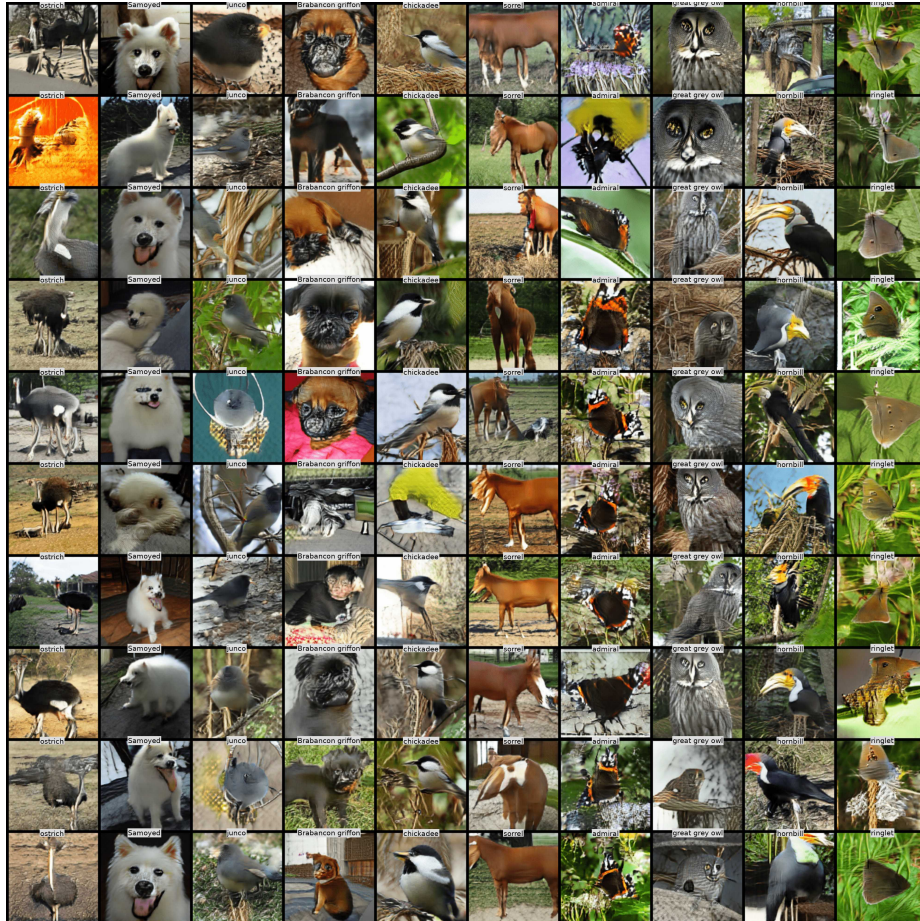


**Fig. 37:** D2M-generated image visualization: ImageNet-D Subset ( $128 \times 128$ ) with IPC1.

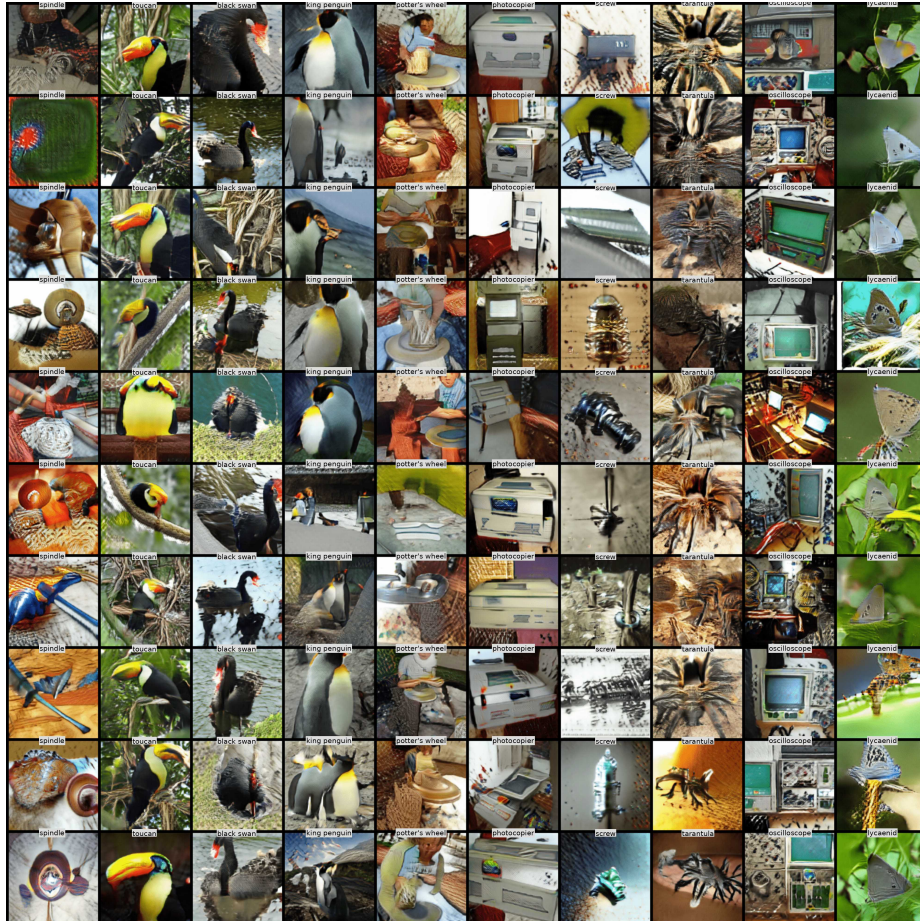


**Fig. 38:** D2M-generated image visualization: ImageNet-E Subset ( $128 \times 128$ ) with IPC1.